ADVANCED SUSTAINABLE SYSTEMS
www.advsustainsys.com

Cellulose-Based Electrolytes in Rechargeable Zn-Battery: An Overview

Jusef Hassoun, Kento Kimura, and Yoichi Tominaga**

Despite commercially diffused as a primary cell, zinc battery is attracting increasing interest as rechargeable system due to its low cost, safety, and environmental sustainability. Furthermore, cellulose-based ion conducting media exploiting solid, jelled, or polymer configurations are well supporting the improvement of this intriguing energy storage system. Here, an overview of recent researches on rechargeable Zn battery, often indicated as Zn-ion battery is reported, exploiting electrolytes using cellulose. It is shown that cellulose-based electrolyte may have either solid, or gel, cross-linked hydrogel, coated, biopolymer, microfibrillated, aligned, amorphous, or self-assembled configurations. In the course of the paragraphs, how the several structural, morphological, and electrochemical studies have clarified fundamental characteristics to allow their operation in battery is revealed. On the other hand, Zn-based energy storage systems are discussed, particularly focusing on Zn–MnO_2, Zn–V_2O_5, and Zn–air as the preferred cell configurations in terms of reliability, electrochemical performances, delivered capacity, and cycling stability. Last but not the least, the review remarks that the cost of these batteries is competitive in the global energy storage market, particularly considering the raw material availability. Therefore, the work sheds light on this dated, while emerging, system of raising interest particularly for stationary storage from discontinuous renewable sources.

1. Introduction

The increasing need for energy triggered the diffusion of alternative sources such as solar, and wind, with consequent raising request for large-scale energy storage to stabilize the grid, while green new deals foreseen the diffusion of electric vehicles powered by batteries and fuel cells.[1–3] Despite the recent progresses and promises,[4] the widely diffused lithium-ion (Li-ion) battery still faces several environmental issues including safety, possible toxicity, recycling, and economic sustainability.[5–7] These challenges may be actually mitigated by developing different battery technologies, e.g., using polysaccharide-based compounds and materials as electrode binders, separators, and gel/solid polymer electrolytes, and different electrochemistry at the electrode side, such as that of the Zn battery as clarified hereafter.[8] Specifically, polysaccharide-based substrates can be proposed as fluorine-free binders or polymer matrixes alternative to polyvinylidene fluoride (PVDF), which is the one typically used in Li battery. Furthermore, the use of nontoxic abundant metals such as Zn, Fe or carbons and oxides can actually represent a step forward for mitigating the impact of toxic and expensive metals such as the cobalt, the use of which is still diffused in Li-battery technology.[5–7]

1.1. The Lignocellulose

Lignin and cellulose, also known as lignocellulose materials, are abundant, renewable, eco-friendly, cost-effective, and possess the right characteristics for being developed into efficient electrochemical energy storage systems. Lignocellulose materials are among the most representative of polysaccharide-based biopolymers available, and they are sufficiently abundant to meet the increasing demand. Furthermore, lignocellulose biopolymers are mechanically flexible, abundant and possess various functional groups, and they may be considered for use in enhanced configurations of electrodes, separators, binders, and electrolytes within sustainable energy-storage devices, such as supercapacitors and batteries.[9] Therefore, the natural biodegradability, renewability, porous structure, good thermal and chemical stability, and

J. Hassoun
Department of Chemical, Pharmaceutical and Agricultural Sciences
University of Ferrara
Via Fossato di Mortara 17, Ferrara 44121, Italy
E-mail: jusef.hassoun@unife.it

J. Hassoun, K. Kimura, Y. Tominaga
Department of Applied Chemistry
Graduate School of Engineering
Tokyo University of Agriculture and Technology
2-24-16, Naka-cho, Koganei-shi, Tokyo 184-8588, Japan
E-mail: ytominag@cc.tuat.ac.jp

K. Kimura, Y. Tominaga
Institute of Global Innovation Research (GIR)
Tokyo University of Agriculture and Technology
2-24-16, Naka-cho, Koganei-shi, Tokyo 184-8588, Japan

The ORCID identification number(s) for the author(s) of this article can be found under https://doi.org/10.1002/adsu.202500287

DOI: 10.1002/adsu.202500287

tunable surface chemistry of lignocellulose triggered the use of functionalized lignocellulose in the electrode materials. Furthermore, the flexibility of this material has allowed the preparation of solid-state or gel electrolytes in combination with various polymers, as well as of sustainable binders or separators. Biodegradability and renewability of lignocellulose is mainly due to its derivation from biomasses (for example, wood or plant seeds), which are periodically regenerated by natural cycles. On the other hand, the porosity of this material is driven from its lignocharacter, which is naturally requested to promote the water uptake of the flora. In addition, the lignocellulose can be combined, rearranged, gelled, or transformed into membranes through various functional groups, such as —OH, —NH_2, —CO, and —COOH, which are naturally linked or artificially included into the structure as illustrated in the subsequent paragraphs.[10] This intriguing substrate acquired largely increasing interest in particular for application in aqueous rechargeable batteries, that appeared so far adequate for the polysaccharide-based biopolymers due to the moderate working voltage. Among these batteries, aqueous rechargeable zinc batteries showed promising features due to the high safety of the metal, its abundance, and environmental compatibility.[11,12]

1.2. The Rechargeable Zinc Battery

Zinc metal has negligible reactivity if compared with alkali metals such as lithium and sodium, with the additional bonus of the limited production costs. This metal has a theoretical specific capacity as high as 820 mAh g^{-1}, and a potential of −0.763 V versus standard hydrogen electrode (SHE), that allowed the development of aqueous electrolytes without relevant hydrogen evolution at basic pH with optimal safety level.[13] Therefore, primary zinc batteries (i.e., piles) in alkaline media have been commercialized by hundreds of thousands of units as systems for powering various electronic devices of common use.[14] However, the nonrechargeable setup hindered the actual use of the alkaline zinc pile for cyclic energy storage, e.g., from renewable sources or in electric vehicles, since this application requires a rechargeable battery in which cathode and anode sides can operate reversibly.[15] Among the cathodes proposed for this scope, manganese oxide has shown the most appealing and reversible activity in aqueous media, with formation of manganese oxyhydroxides or mixed oxides. This electrochemical reaction has been indicated to involve phase changes and concomitant ion exchange, within a potential window extending from ≈0.8 to ≈1.8 V versus Zn^{2+}/Zn.[16] Instead, at the anode side the Zn metal presented various issues ascribed with the possible hydrogen evolution in an acidic condition, and the remarkable tendency to dendrite growth which depended on the characteristic of solid electrolyte interphase (SEI) formed on its surface.[14] In this scenario, the solidified membranes using hydrogel electrolytes appeared as reasonable alternative to overcome the electrolyte loss and limit, at the same time, the dendrite growth at the zinc anode upon repeated stripping/plating due to their elastic characteristics.[17,18] Furthermore, the gelled electrolytes have been indicated to consolidate a stable and durable electrode/electrolyte interphase and a robust SEI layer, even when acid environment was employed in the zinc-ion batteries.[19] Last but not the least, the limited cost of some metals employed at the cathode and anode, e.g., Mn and Zn, compared to metals used in Li-ion cells such as Co, Ni, and Li itself, indicated by the recent estimation of **Figure 1** (left-hand panel), has accelerated the research for these renewed energy storage systems. On the other hand, Zn-ion and Na-ion batteries have comparably low cost and similar energy content of about 100 Wh kg^{-1}, which is rather far from that of Li-ion battery which exceeds 250 Wh kg^{-1}, as shown by the right-hand panel of Figure 1. Therefore, Zn-ion battery has been preferably indicated for use in stationary energy storage rather than electric vehicles.[20,21]

1.3. A Suitable Material Combination

Various studies reported on the use of cellulose-based polymers,[22] modified polymers,[23] doped substrates,[24] hydrogels,[25] separators,[26] biocomposites,[27] and biopolymer gels,[28] for energy storage. The different functional groups mentioned above, which are naturally or synthetically included in these membranes, can facilitate hosting of the Zn^{2+} ions in the backbone and allow the high conductivity by electrostatic interactions due to their polar character. Furthermore, the mild and favorable chemical interaction of these substrates with the Zn metal can ensure a low interphase resistance that typically contributes to the dendrite suppression, thus relevantly improving the cycle life of the Zn-ion cells based on functionalized cellulose substrates. In this scenario, cellulose nanocrystals (CNCs) with different surface functions, charge, and concentrations, have been suggested as a component for battery application.[29] In addition, methyl-cellulose-based solid polymer electrolytes have been proposed with dispersed zinc oxide nanoparticles to promote the use in cell.[30] Among the membranes, multiple cross-linked hydrogel electrolytes have achieved a long lifespan against the Zn metal anode by manipulating desolvation effect and Zn deposition orientation.[31] Interestingly, the dendrite growth on Zn metal anode has been mitigated by using a cellulose-acetate coating integrating ester group with zinc.[32] Furthermore, a dual-cross-linked and self-healable hydrogel electrolyte was suggested for a Zn-ion battery characterized by an improved interfacial ion deposition,[33] while amidoxime functional groups promoted a gel polymer electrolyte (GPE) for aqueous Zn-metal cell.[34] Solid biopolymers based on cellulose acetate (CA) have revealed suitable thermal, structural, and electrochemical characteristics.[35] An adequate ethanol-vapor-induced synthesis of poly(vinyl alcohol) (PVA)/cellulose composite,[36] and the thermoresponsive treatment of carboxymethyl cellulose (CMC) polymer[37] have led to robust solid polymer for Zn-ion battery. Interestingly, aqueous Zn-ion batteries have been proposed with poly(ethylene glycol)/cellulose/$ZnCl_2$ water-in-salt electrolytes,[38] and flexible sustained ionogels with ionic hyperbranched polymers were reported with enhanced ion conduction.[39] Quasi-solid-state Zn-ion batteries have also exploited multifunctional quasigel (QG) layer prepared in situ,[40] and ultrathin natural-cellulose-based hydrogel.[41] Nickel(II) nitrate has been interestingly used as an additive to control the nanoporosity of CA, with water pressure treatment to achieve a highly efficient battery gel,[42] instead cellulose nanofibers (CNFs) subjected to TEMPO

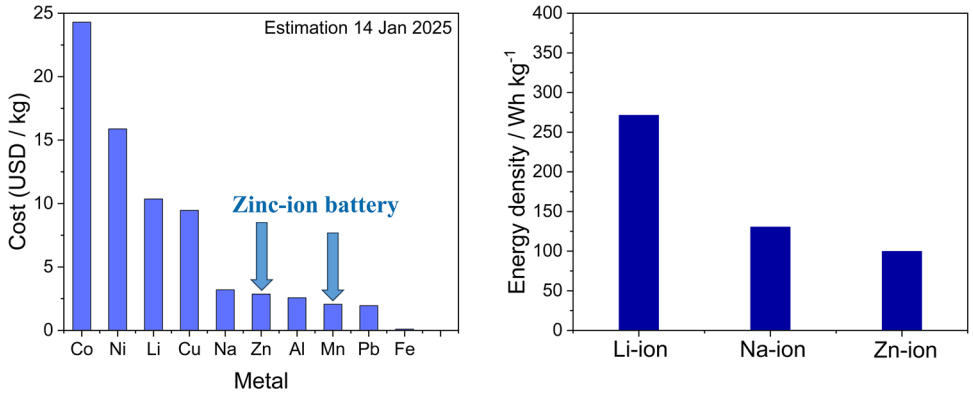

Figure 1. Rough estimation of the row metal price with inset indicating materials typically employed in the Zn-ion battery (left-hand side panel), and comparison of the energy density of Li-ion, Na-ion, and Zn-ion batteries (right-hand side panel).

oxidation chemical fibrillation (TOCNF) produced a hydrogel able to efficiently coordinate Zn^{2+} ions, allowing their mobility in electrolyte projected for rechargeable Zn-ion batteries.[43] Even in the case of the rechargeable Zn–air battery, gel polymer composites with solid-state configuration have been studied as the preferred electrolyte media.[44] Hence, a flexible gel polymer based on CMC blended with PVA or poly(acrylic acid) (PAA) has been developed for rechargeable Zn cell operating in air atmosphere.[45] Another composite GPE for the same battery setup, exploited with success the combination of CMC and PVA,[46] while a biodegradable electrolyte was achieved for flexible Zn–air batteries.[47] Interestingly, the CO_2-retardant effect and the Zn–air battery were exploited at the same time by CO_2 decorating a conductive cellulose electrolyte.[48] On the other hand, composite GPEs based on graphene oxide nanoribbon (GONR) were developed for enhancing mechanical strength and ionic conductivity of flexible Zn–air batteries,[49] and the flexibility of this battery was also enabled by a sodium polyacrylate (PANa)-based gel containing graphene oxide (GO) and CNF.[50] In summary, these synthetic pathways, including various steps of different nature in the aqueous environment, with gelled, polymerized, er solidified state, have well boosted the development of a new generation of Zn-based rechargeable systems. **Figure 2** depicts a selection of the synthetic pathways adopted in the abovementioned researches to achieve cellulose-based electrolyte for energy storage. Indeed, Figure 2a shows the various operating steps for preparation of a cellulose membrane, as well as a photographic image of the obtained membrane before soaking the electrolyte,[41] while Figure 2b reveals a synthesis scheme of polyacrylamide (PAM)–poly(ethylene glycol) diacrylate–CMC (PMC) hydrogel electrolyte.[31] The functional groups–ions interaction in the membranes certainly played a crucial role in stabilizing the cell performances. Some of these interactions are schematically depicted in Figure 2c for a double-network of a CMC/PAM hydrogel membrane,[51] and in Figure 2d for a TOCNF hydrogel electrolyte.[43] On the other hand, nonoptimized aqueous electrolytes can allow dendrite growth at the Zn surface, with passive layer formation and thickening, H_2 evolution, and corrosion during the electrochemical deposition process, as shown by the scheme of Figure 2e.[32] Instead, suitable protection of the Zn, such as by the coating with CA and $Zn(CF_3SO_3)_2$ (CAZ) reported in Figure 2f, can separate the Zn anode and aqueous species in the achieved CAZ@Zn, inhibiting passivation and corrosion, and triggering fast Zn^{2+} diffusion and homogeneous electrochemical deposition without dendrite growth or H_2 evolution.[32] The above illustrated synthetic pathways, as well as the ones in the subsequent paragraphs may actually pave the way for the achievement of rechargeable batteries characterized at the same time by low economical impact and relevant environmental sustainability, thus allowing their large-scale diffusion as alternative to the most widespread rechargeable system. A proof of the improvement achieved by the use of the membranes based on cellulose for battery application is represented in **Figure 3**, which reports the Zn^{2+} plating/stripping voltage profiles in Zn/Zn symmetric cells using some of the various electrolyte samples already illustrated in Figure 2.

Indeed, the cell in Figure 3a was tested at the current density of 1 mA cm^{-2} at areal capacity of 1 mAh cm^{-2} (magnification in Figure 3b) showing a substantial voltage increase for the glass fiber membrane, ranging from 180 to 260 mV over a span of 90 h due to uneven Zn deposition and the formation of a wide solid electrolyte interface, and abrupt polarization voltage drop to zero upon 120 h due to zinc dendrites penetrating the glass fiber membrane, resulting in direct electrical contact between the two electrodes with short circuit. Instead, the cell using cellulose membrane exhibited much smaller and relatively stable polarization (30 mV at 1500 h) without significant fluctuations due to improved interfacial compatibility between the electrode and electrolyte. The slight increase in polarization from 1500 to 1800 h has been attributed to electrolyte volatilization, within the cell.[41] Furthermore, the cell with PMC hydrogel electrolyte in Figure 3c revealed a cycling stability extended for 5000 h at a current density of 1.0 mA cm^{-2} and a capacity density of 1.0 mAh cm^{-2}. By contrast, the cell with the $ZnSO_4$ reference aqueous electrolyte evidenced an increasing polarization around 150 h, and short circuit around 160 h, for the same reasons illustrated above.[31] Figure 3d depicts for the symmetric cell at 0.2 mA cm^{-2} with PAM hydrogel electrolyte stable trend only until 200 h and subsequent deterioration, while the cell with CMC/PAM hydrogel electrolyte operated without any short circuit or obvious overpotential rise of over 400 h, thus suggesting significantly improved interfacial stability between CMC/PAM hydrogel electrolyte and Zn.[51] On the other hand, the cell in

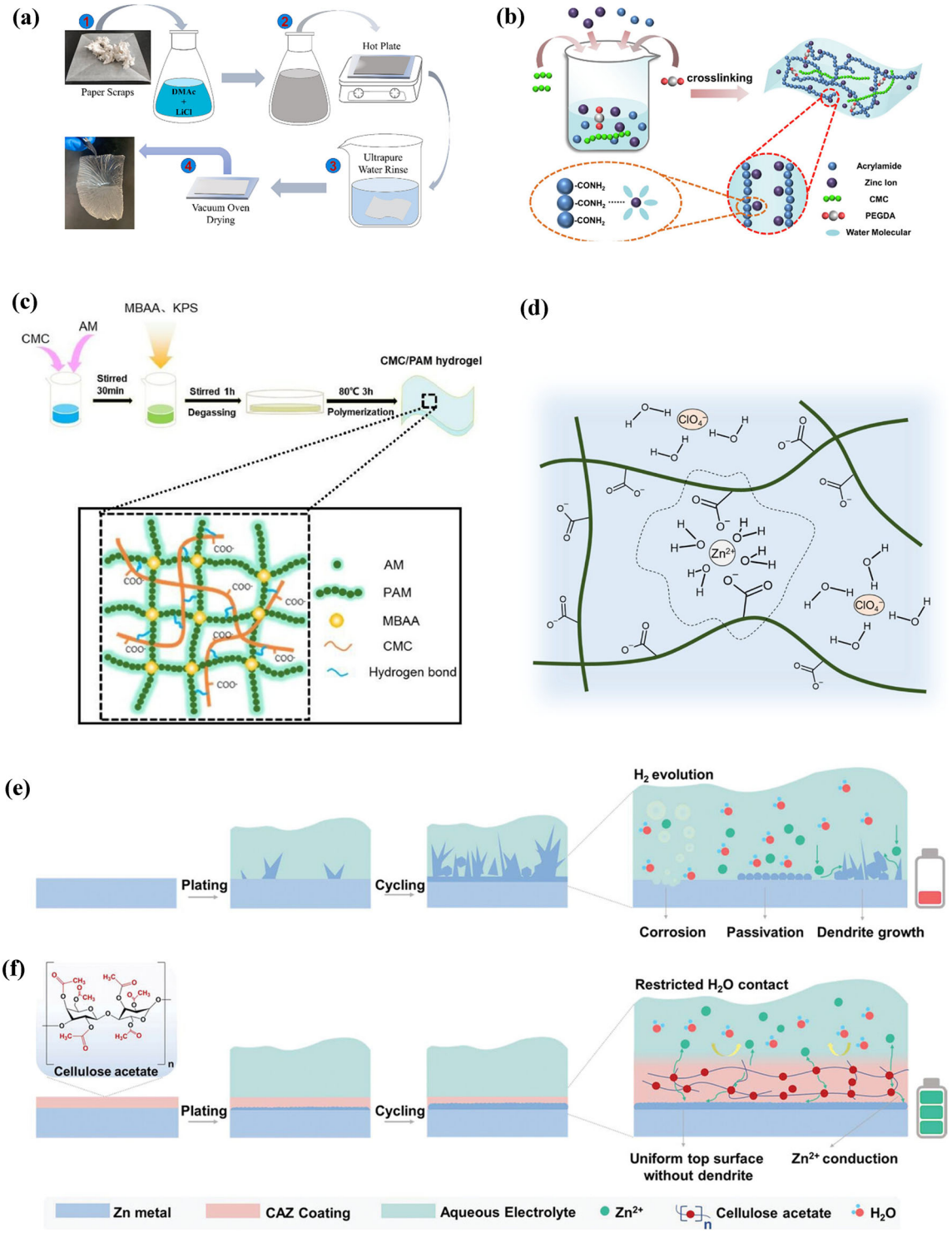

Figure 2. a) The preparation process of cellulose-based membranes. The bottom-left picture in this panel is a photograph of the obtained cellulose membrane before soaking the electrolyte. Adapted with permission.[41] Copyright 2023, Elsevier. b) Synthetic schematic diagram of PMC hydrogel electrolyte. Adapted with permission.[31] Copyright 2022, Elsevier. c) Illustration of the double-network of CMC/PAM hydrogel. Adapted with permission.[51] Copyright 2021, Elsevier. d) Schematic illustration of the expected internal interaction structures in the TOCNF hydrogel electrolyte. Adapted with permission.[43] Copyright 2024, RSC. e,f) Schematic diagrams of the metal deposition processes on bare and CAZ coated Zn. (e) Dendrite growth, passive layer formation, H_2 evolution, corrosion, and passive layer growth during the electrochemical deposition process on bare Zn surface in an aqueous electrolyte. (f) The CAZ with high ionic conductivity can separate the Zn anode and aqueous species in the CAZ@Zn, inhibiting passivation and corrosion and guaranteeing fast Zn^{2+} diffusion and homogeneous electrochemical deposition without dendrite growth and H_2 evolution. Adapted with permission.[32] Copyright 2022, Wiley. See Table 1 for acronyms' summary.

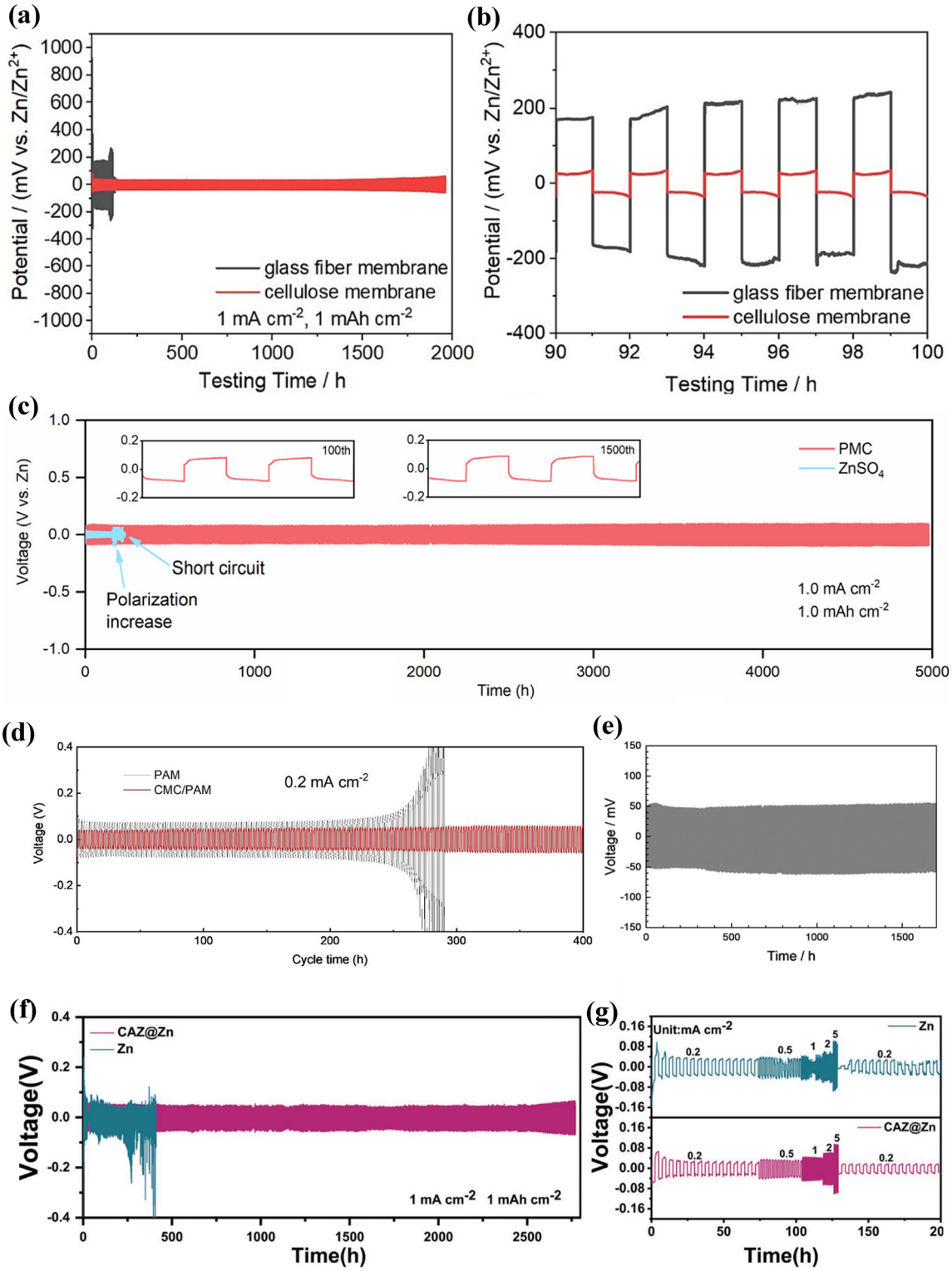

Figure 3. The Zn^{2+} plating/stripping voltage profiles in Zn/Zn symmetric cells assembled using some of the membranes illustrated in Figure 2. a,b) Cells with cellulose membrane or glass fiber membrane (a) at the current density of 1 mA cm^{-2} at areal capacity of 1 mAh cm^{-2}, and (b) the corresponding magnification. Adapted with permission.[41] Copyright 2023, Elsevier. c) Cells with PMC hydrogel electrolyte and $ZnSO_4$ reference solution. Adapted with permission.[31] Copyright 2022, Elsevier. d) Cells using CMC/PAM hydrogel electrolyte and PAM hydrogel electrolyte at 0.2 mA cm^{-2}. Adapted with permission.[51] Copyright 2021, Elsevier. e) Cell using the TOCNF hydrogel electrolyte. Adapted with permission.[43] Copyright 2024, RSC. f,g) CAZ@Zn symmetrical cells at (f) 1 mA cm^{-2} with capacity of 1 mAh cm^{-2}, and (g) the corresponding rate performance. Adapted with permission.[32] Copyright 2022, Wiley. See Table 1 for acronyms' summary.

Figure 3e using the TOCNF hydrogel electrolyte revealed gradual increase of the overpotential to 53 mV during the initial 50 h, and a subsequent decrease to 48 mV and stabilization to values between 48 and 54 mV held through the whole test exceeding 1500 h. This behavior suggested the growth of suitable passivating SEI during the initial stage, a subsequent stabilization, and partial dissolution with decrease of the electrode/electrolyte interphase resistance.[43] Interestingly, the CAZ@Zn/CAZ@Zn symmetrical cell was cycled both at a constant current of 1 mA cm^{-2} with capacity of 1 mAh cm^{-2} in Figure 3f, and at various current rates in Figure 3g.[32] After 30 h at 1 mA cm^{-2} (Figure 3f), the potential of the bare Zn/Zn cell suddenly fallen down due to a "soft short."

The above soft short consisted of small localized electrical contact between two Zn electrodes, due to the dendrite growth toward the opposing electrode after penetrating the glass fiber separator and its subsequent dissolution, allowing the charging/discharging process to proceed however less stably. The slow increase of the potential was ascribed due to gradual increase in internal resistance, induced by dendritic growth caused by unequal zinc deposition, and after 420 h of operation, the symmetric Zn/Zn battery failed. By contrast, the symmetric CAZ@Zn/CAZ@Zn battery well operated over 2800 h with a low overpotential due to the homogeneous Zn deposition with low interfacial resistance and without dendrites. The comparison of the rate performance of symmetrical cells using either CAZ@Zn or bare Zn (Figure 3g) revealed soft shorts and higher voltage hysteresis for the former than the latter, especially at high current densities, suggesting favorable stability of the CAZ@Zn anode.[32] Overall, Figure 3 well indicates a notable improvement of the cycling stability of the anode side promoted by the use of the cellulose-based membranes, in particular for those in which the water content is limited and the mechanical stability improved.

1.4. Subdivision of This Review

Subsequently to the previous paragraphs describing various pathways for cellulose-based membrane preparation, battery application, and possible combinations, the next ones will show selected examples of rechargeable Zn cells which have been categorized for convenience in this review by three main classes, i.e., i) zinc–manganese oxide battery, ii) zinc–vanadium oxide battery, and iii) zinc–air battery. Although different categorization may be made, this selection appeared to us the most convenient one for taking into account at the same time the process scalability, the state of the art of rechargeable Zn cells, and their best performances in literature. This comparison is reported with the aim of achieving a valid benchmark in terms of energy density and cycle life to consider possible practical application of the Zn battery for sustainable energy storage. On the other hand, the material availability, modest expected cost, and suitable features of the cells can trigger further research and development of this intriguing system to allow its final use for selected sectors, such as the energy storage from discontinuous renewable energy sources. For reader's convenience, we summarized all the acronyms, specified at their first appearance in the text, also in the **Table 1**.

Table 1. Summary of the acronyms reported in this review and the corresponding extended versions.

Acronym	Extended version
PVDF	Polyvinylidene fluoride
GPE	Gel polymer electrolyte
CV	Cyclic voltammetry
EIS	Electrochemical impedance spectroscopy
SHE	Standard hydrogen electrode
SEI	Solid electrolyte interphase
CNC	Cellulose nanocrystals
CMC	Carboxymethyl cellulose
PAM	Polyacrylamide
PMC	PAM—poly(ethylene glycol) diacrylate—CMC
CNF	Cellulose nanofibers
TOCNF	TEMPO-oxidized CNF
CA	Cellulose acetate
CAZ	CA—$Zn(CF_3SO_3)_2$
COP	Covalent organic polymer
QG	Quasigel
AO	Amidoximation
PIM	Polymer of intrinsic microporosity
BC	Bacterial cellulose
DES	Deep eutectic solvents
SA	Sodium alginate
ORR	Oxygen reduction reaction
OER	Oxygen evolution reaction
GO	Graphene oxide
PANa	Sodium polyacrylate
GONR	Graphene oxide nanoribbons
PAA	Poly(acrylic acid)
PVA	poly(vinyl alcohol)
PVAA	PAA—PVA
SSE	Solid state electrolyte
CC—CO_2	CO_2-bedecked cellulose
QSPI	Quaternized soybean protein isolate
HEC	Highly hydrophilic polymer hydroxyethyl cellulose
DMAc	N,N-dimethyl acetamide
RCT	Charge transfer resistance

2. Zinc–Manganese Oxide Rechargeable Batteries

Zinc–manganese oxide battery is one of the most promising rechargeable system among the various proposed ones, and its electrochemistry has been well studied since the introduction of the primary system (e.g., zinc–carbon alkaline battery), until the development of the reversible version of the cell by adopting a suitable setup of cathode and electrolyte media. Manganese oxide (predominantly MnO_2) reacts in a Zn-ion battery with a mechanism depending on the electrolyte condition, in general leading to a voltage signature extending from about 1 to 1.6 V versus Zn^{2+}/Zn, and a theoretical specific capacity of 308 mAh g^{-1} as referred to the MnO_2 weight. Therefore, in neutral condition, Zn^{2+} dissolves from the anode in discharge potentially forming $Zn(OH)_2$ that can possibly precipitate in part at the surface.

The Zn^{2+} ions can also insert in the MnO_2 cathode tunnels according to the reaction[52]

$$Zn^{2+}+2e^{-}+2MnO_2 \leftrightarrows ZnMn_2O_4 \quad (1)$$

Hence, MnO_2 tunneled structure (hollandite-etype phase) changes to spinel-like trivalent manganese phase ($ZnMn_2O_4$), then into layered divalent manganese phase (Zn_xMnO_2, $x < 0.5$), and finally to tunneling divalent manganese phase (Zn_xMnO_2, $1 > x > 0.5$) during discharge.[53] Three Mn ions coexist after discharge, and the interconversion of Mn^{4+}, Mn^{3+}, and Mn^{2+} allows the energy conversion.[54] Instead, in alkaline electrolytes $Zn(OH)_2$ is formed certainly at the anode, and conversion reaction can occur at the cathode according to mechanism involving OH^- ions as follow[55]

$$2MnO_2 + 2H_2O + 2e^- \leftrightarrows 2MnOOH + 2OH^- \quad (2)$$

In the latter case, OH^- ions can also form the complex $[Zn(OH)_4]^{2-}$ at the electrodes surface and limit the long-term reaction reversibility, thus suggesting electrolyte change to slightly acidic condition for increasing the lifespan of the cell.[56]

On the other hand, in acidic condition the reaction at the cathode side is

$$MnO_2 + H^+ + e^- \leftrightarrows MnOOH \quad (3)$$

which may be followed by the process

$$MnOOH + 3H^+ + e^- \leftrightarrows Mn^{2+}+2H_2O \quad (4)$$

Increasing the H^+ concentration can improve MnO_2 discharge, however it can also lead to parasitic reactions at the Zn anode, such as corrosion of Zn metal in discharge or H_2 gas production during charge.[53] Therefore, the electrolyte medium should be tuned ad hoc to allow the reversible Zn stripping/deposition at the anode side and, at the same time, guarantee a reversible reaction at the MnO_2 cathode side. Lignocellulose-based electrolytes, typically functionalized with suitable groups, such as carboxyl, hydroxyl, ammine, or ether, actually allowed the development of efficient Zn–MnO_2 rechargeable batteries. In this regard, a literature work reported in situ building of a multifunctional QG layer for protecting the zinc anode and allowing the aqueous Zn battery to operate for long cycling.[40] The authors solved the issues of dendrite, corrosion, and H_2 evolution by preparing in situ a hydrophilic layer, consisting of a covalent organic polymer (COP) and CMC, to construct a multifunctional QG interface between Zn metal and the electrolyte. This COP—CMC/QG interface significantly improved the rechargeability of the Zn anode through enhancing Zn^{2+} transport kinetics, and guiding uniform nucleation. **Figure 4a** reports a schematic diagram of COP—CMC/QG formation and Zn plating on bare Zn and COP—CMC—Zn. The COP—CMC—Zn anode exhibited overpotential of 12 mV at 0.25 mA cm^{-2}, with cycle life over 4000 h at the same current and 2000 h at 5 mA cm^{-2} in symmetrical cells. Figure 4b depicts the voltage profiles Zn/MnO_2 full cells with bare Zn and coated Zn at a current density of 0.3C (1C = 308 mA g^{-1}, based on MnO_2), while Figure 4c shows the related cycling performance at a current of 5C. The cell using the coated Zn operated with an average working voltage of 1.4 V and a capacity of about 150 mAh g^{-1} for 1000 cycles, while the cell using bare Zn revealed a substabtial decay over the same cycling stage.[40] Another work hindered the dendrite growth on the zinc anode by using amidoxime functional groups in GPE.[34] A membrane has been prepared by introducing polymers of intrinsic microporosity (PIMs) subjected to amidoximation (AO-PIM-1) with bacterial cellulose (BC), to achieve the AO-PIM-1/BC GPEs. In this GPE, the C═N in the amidoxime functional group coordinated Zn^{2+} to promote the ion transport, as well as uniform deposition of Zn. In addition, the hydrophilic groups —NH_2 and —OH reduced the energy required for the desolvation of hydrated Zn^{2+}. Molecular dynamics simulations were used to evaluate the interaction of hydroxyl, ammine, and C═N groups with Zn^{2+}. In bare electrolyte, Zn^{2+} was closely surrounded by six H_2O molecules forming the octahedral $[Zn(H_2O)_6]^{2+}$, the large size of which hindered the desolvation. Instead, the hydrophilic functional groups —NH_2 and —OH in the AO-PIM-1 framework altered the hydration structure and reduced the energy required for dissolution. Hence, the C═N bond became the transport site for Zn^{2+}, and the desolvation energy resulted lower in AO-PIM-1 than PIM-1. In addition, the amidoxime functional groups adsorbed triflate anion (OTF^-), which further promoted the transfer of Zn^{2+}. The model indicated an average coordination number of H_2O molecules around Zn^{2+} of 3.08 in the AO-PIM-1 framework, rather than 3.86 in the PIM-1 structure. This decrease in the water coordination number suggested a reduction in the desolvation energy. Consequently, deposition of Zn was considered more uniform in AO-PIM-1 than in PIM-1. This finding confirmed that the presence of C═N group in the AO-PIM-1 can provide transport sites for Zn^{2+} binding, thereby reducing the hydration coordination number of Zn^{2+}, and promoting uniform deposition of the Zn anode. Accordingly, the scheme of Figure 4d depicts the regulation of the Zn anode mechanism by PIMs. Hence, Zn/Zn symmetrical cells with the AO-PIM-1/BC GPE exhibited a cycle life extended to 1100 h. The Zn/α-MnO_2 battery prepared using the GPE retained 85% of its initial capacity of 120 mAh g^{-1} after 400 cycles at 0.5C (Figure 4e).[34] A TOCNF hydrogel electrolyte has been also set as simple approach for rechargeable Zn-ion batteries (see scheme in Figure 2d for related ion–gel interactions).[43] The hydrogel using both Zn perchlorate and sulfate, was a nonflowable solid-like with strong shear-thinning behavior. The Zn-ion–gel battery with a β-MnO_2 cathode showed a working potential of 1.4 V versus Zn^{+2}/Zn by cyclic voltammetry (CV) in Figure 4f, an activation process after the first cycle leading to resistance decrease evidenced by electrochemical impedance spectroscopy (EIS, Figure 4g), and delivered a capacity over 120 mA h g^{-1} allowing safe energy storage, with cycle life promoted by changing the salt from $Zn(ClO_4)_2$ to $ZnSO_4$ (see cycling test in Figure 4h).[43]

On the other hand, a quite robust gel electrolyte has been developed by ethanol-vapor-induced method for flexible Zn-ion battery.[36] This process, schematized in **Figure 5a**, has foreseen the use of cellulose/deep eutectic solvent (DES) molecular system, and was indicated to speed up hydrogen bonding and ion-complexation with Zn^{2+}, resulting into a mechanical strength of 0.88 MPa (see photographic image), cathion transference number of 0.7, and ionic conductivity of 8.39 mS cm^{-1}. Figure 5b shows the charge–discharge curves at different bending angles

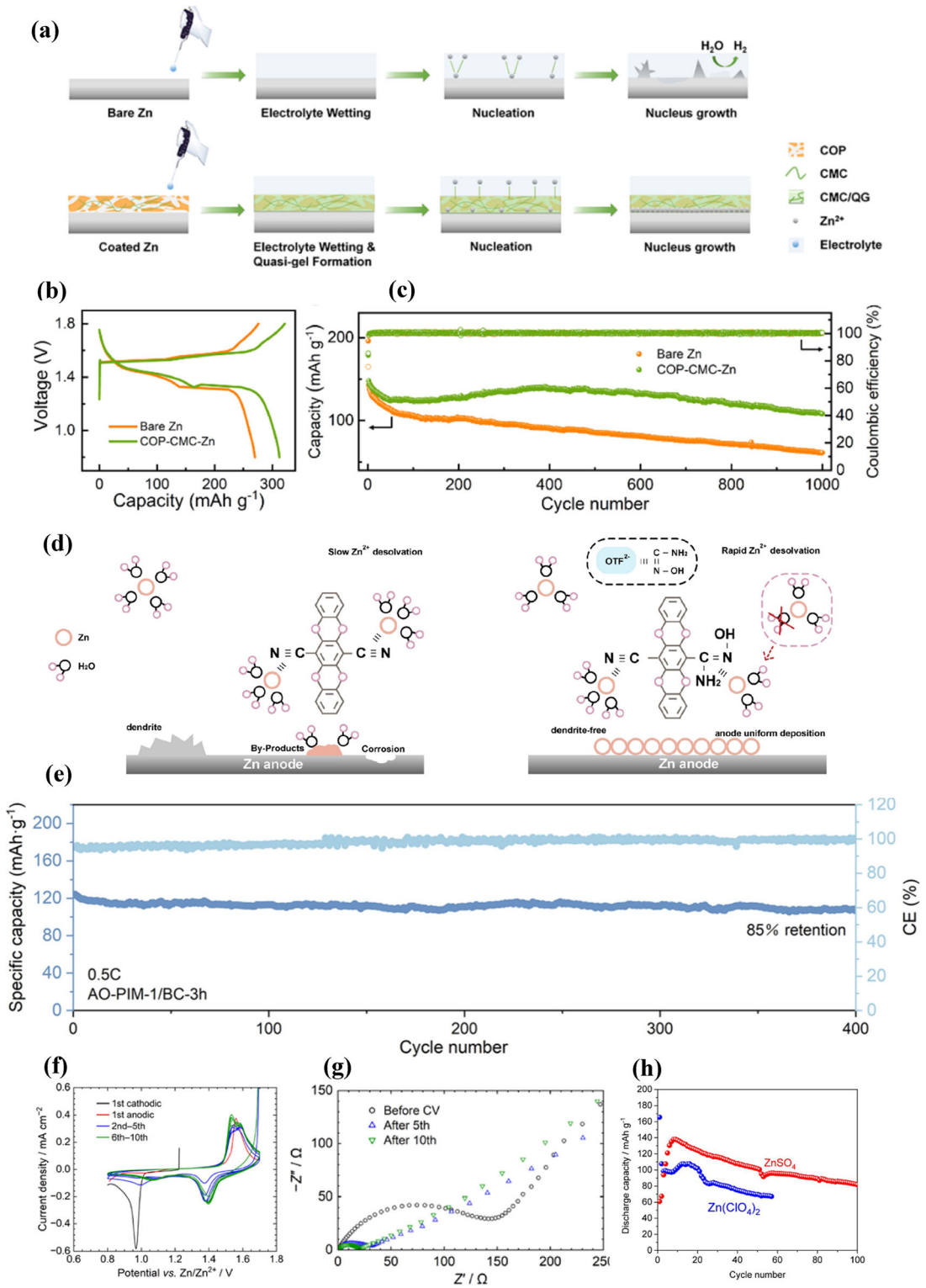

Figure 4. a–c) Characteristics of COP and COP—CMC/QG GPE for Zn anode. (a) Schematic diagram of COP—CMC/QG formation and Zn plating on bare Zn and COP—CMC—Zn. (b) Voltage profiles of Zn/MnO_2 full cells with bare Zn and coated Zn at a current density of 0.3C (1C = 308 mA g^{-1}, based on MnO_2). (c) Cycling performance at a current density of 5C. Adapted with permission.[40] Copyright 2021, ACS. d,e) Characteristics of GPEs with PIMs. (d) Schematic diagram of the regulation of the Zn anode mechanism by PIMs. (e) Zn/α-MnO_2 cell long cycling performances at 0.5C. Adapted) with permission.[34] Copyright 2024, Elsevier. f–h) Electrochemical performances of Zn/MnO_2 cell with TOCNF hydrogel electrolyte. (f) CV curves, (g) impedance spectra using $Zn(ClO_4)_2$ salt, and (h) capacity trends of galvanostatic cycling tests at C/20 using two different salts at 25 (1C = 308 mAh g^{-1}). Adapted with permission.[43] Copyright 2024, RSC. See Table 1 for acronyms' summary.

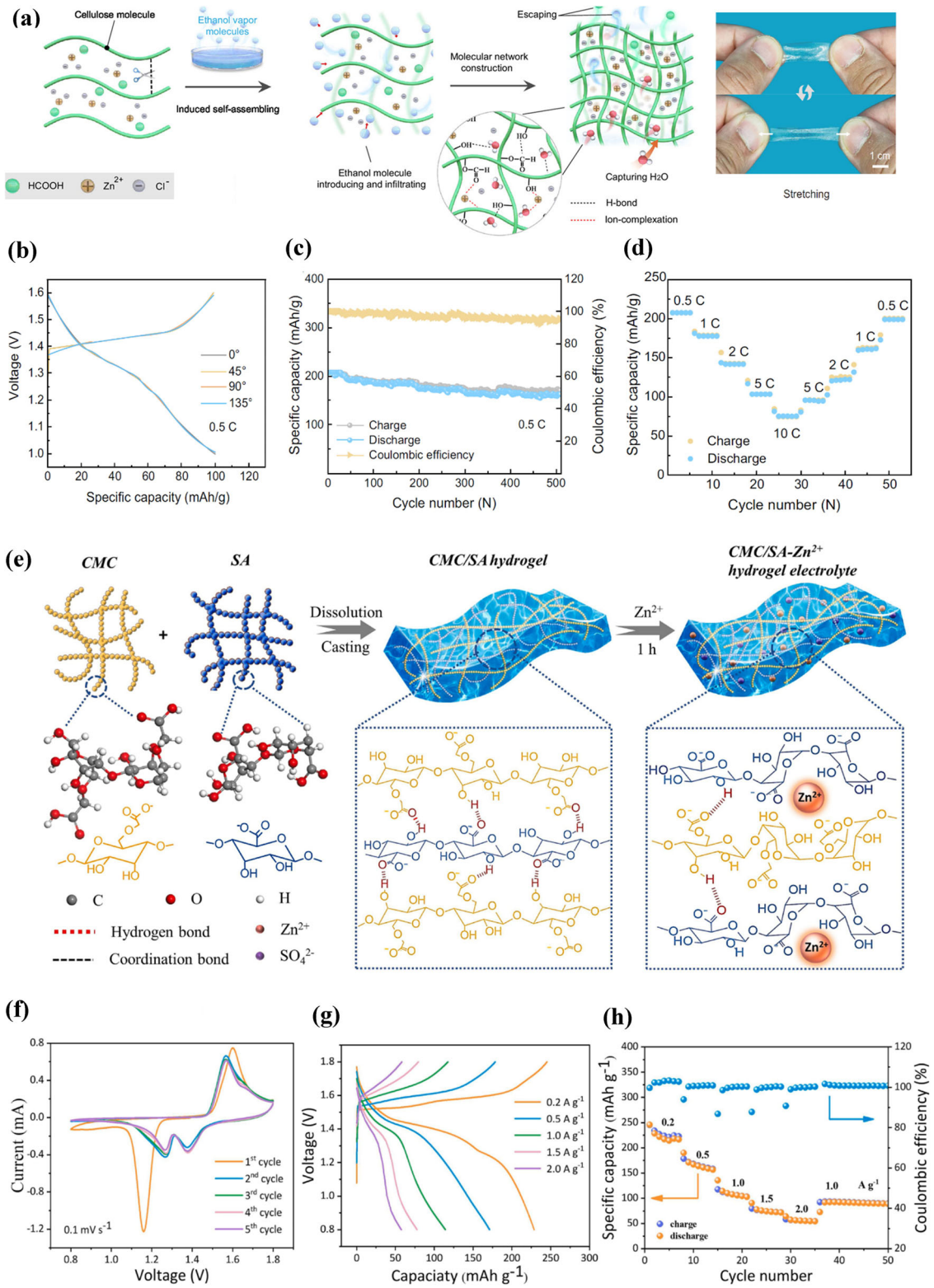

Figure 5. a) Mechanism of ethanol-vapor-induced preparation of Zn–gel from DES molecular system, and a photograph of the membrane. b) Charge–discharge curves at different bending angles of a Zn–gel/carbon cloth@MnO_2 (CC@MnO_2) battery. c) Cyclic performance test of flexible battery at 0.5 C, and d) rate capability of the at varied current densities from 0.5 to 10 C. Adapted with permission.[36] Copyright 2024, Wiley. e) Synthesis schematic of the CMC/SA—Zn^{2+} hydrogel electrolyte. f) CV curves at 0.1 mV s^{-1}. g) Galvanostatic cycling discharge curves and h) rate performance of the Zn–MnO_2 batteries with CMC/SA—Zn^{2+} hydrogel electrolyte at room temperature. Adapted with permission.[33] Copyright 2024, Elsevier. See Table 1 for acronyms' summary.

of a Zn–gel/carbon cloth@MnO_2 battery, revealing its notable flexibility. This battery has been cycled with an average voltage of 1.3 V, reversible capacity of about 200 mAh g^{-1} over 500 cycles (Figure 5c), and a rate capability extending from 0.5 to 10 C with a residual capacity of 75 mAh g^{-1} at the higher C-rate (Figure 5d).[36] With the aim of further improving the interfacial ion deposition in Zn battery, and at the same time the mechanical features, dual-cross-linked hydrogel electrolyte has been prepared (scheme in Figure 5e).[33] The cross-linked self-healing hydrogel electrolyte, including sodium CMC, sodium alginate (SA) and Zn^{2+} (CMC/SA—Zn^{2+}), has been projected for flexible Zn–MnO_2 battery that can recover electrochemical performance even after multiple damages for use in wearable electronics. The metal coordination interactions of carboxyl groups with Zn^{2+}, depicted in scheme, contributed to the mechanical and electrochemical properties of CMC/SA—Zn^{2+} hydrogel, and improved the compatibility with the electrode, thus resulting in efficient Zn deposition. Reversible plating/stripping performance has been observed in a symmetric cell for 2000 h, and a flexible Zn–MnO_2 battery has been achieved operating from 1.2 to 1.4 V (voltammetry in Figure 5f), and delivered capacity ranging from about 220 to 50 mAh g^{-1} depending on the employed current (Figure 5g,h).[33] Finally, a modified hydrogel has been designed as the electrolyte to induce the zinc deposition without dendrite formation at the metal anode.[51] In the above research, a CMC/PAM hydrogel has been prepared by introducing double-network structure to improve the mechanical properties of the electrolyte. The electrostatic interaction between carboxyl groups and Zn^{2+} induced the deposition of zinc ions on the electrode surface, leading to remarkable reversibility and stability (see Figure 2c and Figure 3d).

The CMC/SA—Zn^{2+} hydrogel electrolyte has been used in flexible Zn–MnO_2 battery operating from 1 to 1.4 V, with capacity ranging from 250 to 70 mAh g^{-1} depending on the current rate, and a long range cycling with capacity of 150 mAh g^{-1} retained over 90% for 500 cycles at 0.3 mA cm^{-2}.[51]

In summary, the example reported above well indicate that the combination between polymer electrolytes based on cellulose, improved Zn, and MnO_2 electrodes can actually allow reversible energy storage systems with long lifespan and relevant performances.

3. Zinc–Vanadium Oxide Rechargeable Batteries

Vanadium oxide structure has been defined as highly adaptable to the accommodation of various cations, including Zn^{2+}, due to the deformability of the V—O polyhedra and the variable valence of vanadium.[57] Therefore, various vanadates with different M—V—O structures (where M can by a metal ion or NH^{4+}) have been proposed as the cathode materials.[58] Among them, V_2O_5 or MV_xO_y have been vastly employed in lithium and sodium storage systems. Regarding Zn^{2+} ion intercalation in V_2O_5, one of the typical proposed representatives was $Zn_{0.25}V_2O_5{\cdot}nH_2O$.[59] Various research papers have demonstrated that the addition of cations can provide excellent electrochemical properties to vanadates, and enhance in addition the ion intercalation kinetics.[60] Therefore, the introduction of metal ions has so far produced vanadates with different crystal structures and electrochemical characteristics. Typically, the reaction of V_2O_5 in Zn battery foresees insertion of Zn^{2+} into the vanadate structure, within a vast potential range extending from 0.3 to 1.6 V versus Zn^{2+}/Zn

$$V_2O_5 + xZn^{2+} + 2xe^- \leftrightarrows Zn_xV_2O_5 \quad (5)$$

This reaction also includes the appearance of the new hydrated phases, caused by the improved binding energy between the Zn^{2+} embedded into the V_2O_5 layer and H_2O.[61] Depending on the electrolyte, the electrochemical reaction may also follow the mechanism

$$V_2O_5.nH_2O + 2Zn^{2+} + 4e^- \rightarrow Zn_2V_2O_5 \cdot nH_2O \quad (6)$$

The generation of a new hydrated phase may occur also during this reaction.[62] Therefore, the selection of electrolytes with adequate functional groups, such as the ones characteristic of the lignocellulose derivatives, gels, membranes, and polymers, can play a key role in enabling reversible and efficient electrochemical process at the cathode, and for ensuring at the same time an efficient and smooth metal deposition at the Zn anode. In this regard, a cellulose-acetate coating has been performed by integrating ester group to the Zn salt to limit the dendrite formation on the Zn metal anode.[32] Hence, ion-affiliative CAZ coating has been made on Zn anode (CAZ@Zn) to exploit the complexation effect between the polar ester group and Zn^{2+} (see Figure 2f). The CAZ polymer coating enhanced the hydrophilicity of the Zn anode and reduced the interfacial resistance, allowing rapid Zn^{2+} diffusion to get homogeneous Zn deposition and suppress dendrite formation. The symmetric CAZ@Zn/CAZ@Zn cell demonstrated reversible plating/stripping over 2800 h at 1 mA cm^{-2}, as already shown in Figure 3f, while CAZ@Zn battery with the $NH_4V_4O_{10}$ cathode achieved more stable performance than that of bare Zn. CV indicated a wide working potential range, with peaks extending from 1.3 to 0.4 V versus Zn^+/Zn (**Figure 6a**), reflected into the specific capacity versus voltage curves at various current densities in Figure 6b,c, with similar polarization of the cell using the CAZ@Zn and bare Zn, and an average working voltage of 0.8 V. On the other hand, the rate performance (Figure 6d) evidenced a better response of the cell using CAZ@Zn, and a delivered capacity ranging from 400 mAh g^{-1} at 0.1 A g^{-1}, and 60 mAh g^{-1} at 5 A g^{-1}. Furthermore, the cycling performance of the cells at 1 A g^{-1} (Figure 6e) showed the most relevant differences between CAZ@Zn and bare Zn, with a capacity of 170 mAh g^{-1} retained for 2000 cycles for the former and much faster decay for the latter.[32] A natural-cellulose-based hydrogel membrane has been made with ultrathin flat structure using paper scraps as raw material in N,N-dimethyl acetamide (DMAc)/LiCl dissolution system (see preparation process in Figure 2a).[41] The cellulose membrane has shown a high liquid absorption ability and favorable mechanical properties, ion conductivity of 0.643 mS cm^{-1}, electrochemical stability over 1.6 V, and a activation energy for Zn^{2+} conduction of 3.2 kJ mol^{-1}. The Zn/Zn symmetric cell assembled with the cellulose hydrogel exhibited reversible Zn^{2+} stripping/plating prolonged over 1800 h at 1 mA cm^{-2}, as already reported in Figure 3a, while the chronoamperometry profiles of the same cell at room temperature (Figure 6f) suggested fast Zn^{+2}-ion transfer, with a mechanism supported by the —OH functional groups of the membrane, as schematized in Figure 6g. The cyclic performances of the Zn/cellulose

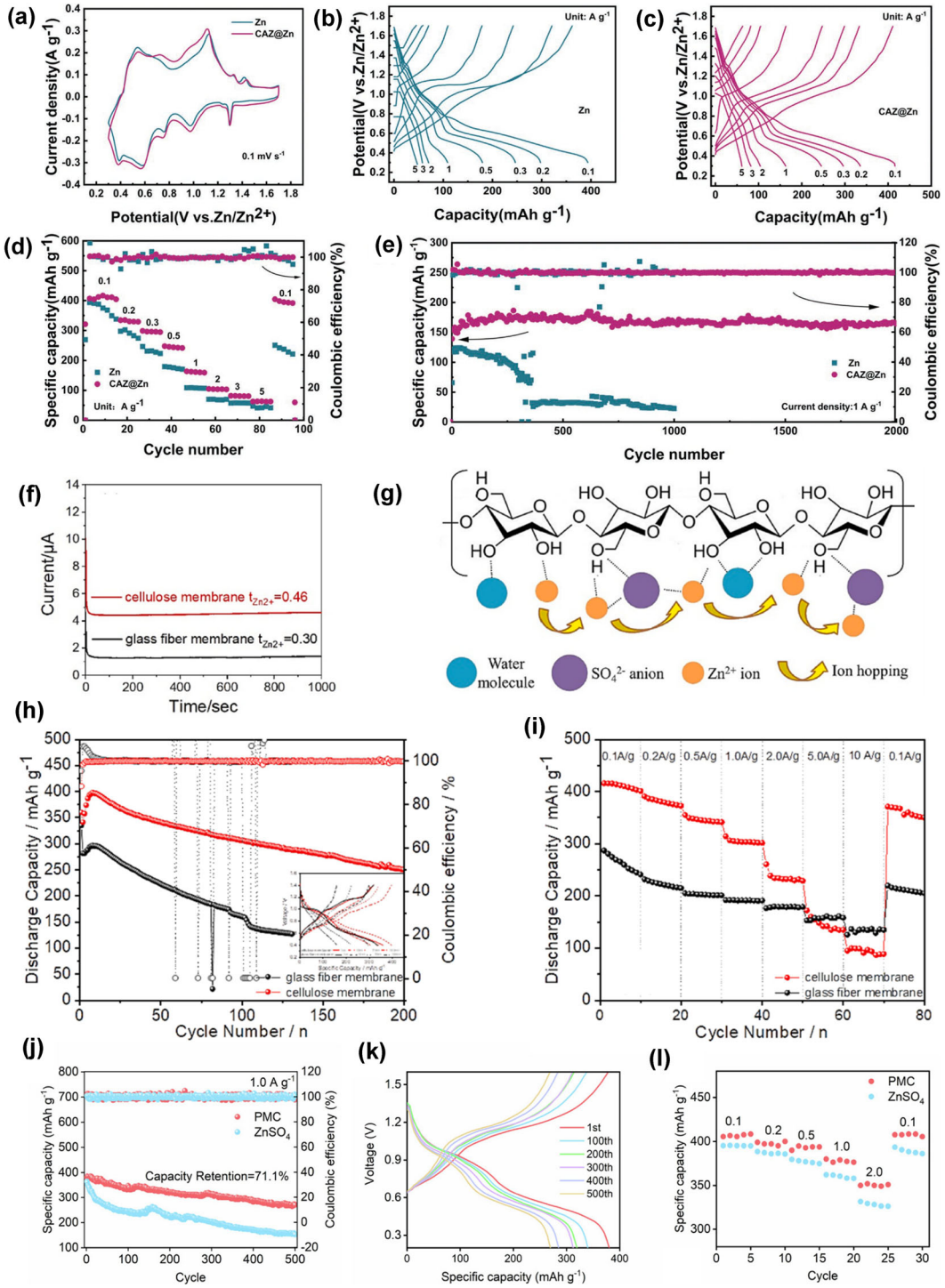

Figure 6. a–e) Performances of CAZ@Zn in battery (a) CV of $Zn/NH_4V_4O_{10}$ and $CAZ@Zn/NH_4V_4O_{10}$ cells at 0.1 mV s^{-1}, (b, c) specific capacity/voltage curves at various current densities, (d) rate performance, and (e) cycling performance of the cells at 1 A g^{-1}. Adapted with permission.[32] Copyright 2022, Wiley. f–i) Ultrathin natural-cellulose-based hydrogel membrane and Zn/V_2O_5 battery. (f) Chronoamperometry profiles for the cellulose membrane and glass fiber membrane in the Zn/Zn symmetric cells at room temperature with a step potential of 10 mV. (g) Scheme of Zn ion transfer mechanism in the cellulose hydrogel electrolyte. (h) Cyclic performances of the Zn/cellulose membrane/V_2O_5 cell and Zn/glass fiber membrane/V_2O_5 cell at 0.1 A g^{-1}. (i) Rate performances of the Zn/cellulose membrane/V_2O_5 cell and Zn/glass fiber membrane/V_2O_5 cell. Rate performance, and (e) cycling performance of the cells at 1 A g^{-1}. Adapted with permission.[41] Copyright 2023, Elsevier. j–l) Application of PMC hydrogel electrolyte in Zn/V_2O_5 battery. (j) Cycle performance of Zn/V_2O_5 batteries with different electrolytes (current density: 1.0 A g^{-1}); (k) Voltage/capacity diagram at 1.0 A g^{-1} of Zn/PMC hydrogel/V_2O_5 battery, and (l) rate capability of Zn/V_2O_5 batteries assembled with bare and PMC hydrogel electrolytes. Adapted with permission.[31] Copyright 2022, Elsevier. See Table 1 for acronyms' summary.

membrane/V_2O_5 cell at 0.1 A g^{-1} (Figure 6h) revealed a capacity from 400 to 250 mAh g^{-1} over 200 cycles at an average voltage of 0.8 V (inset), exceeding the performances of the and Zn/glass fiber membrane/V_2O_5 bare cell which delivered from 300 to 150 mAh g^{-1} for less than 150 cycles. Furthermore, the rate performances of the Zn/cellulose membrane/V_2O_5 cell exceeded the one of Zn/glass fiber membrane/V_2O_5 cell until a current of 2 A g^{-1} (Figure 6i), with a capacity from 400 mAh g^{-1} at 0.1 A g^{-1} to 250 mAh g^{-1} at 2 A g^{-1}.[41] Multiple cross-linked hydrogel electrolytes have been exploited for manipulating desolvation effect and Zn deposition orientation, and used in a Zn battery operating with the V_2O_5 cathode.[31] The hydrogel was based on the already described PMC (see Figure 2b), and was designed to reduce the desolvation energy barrier of Zn and orientate its deposition. The zinc desolvation activation energy in the PMC hydrogel electrolyte was deducted theoretically and experimentally to be much lower than that of conventional aqueous electrolyte, due to the tuned Zn^{2+} solvation structure. Based on the high binding energy between amide groups and Zn^{2+}, the polymer chains in PMC acted as Zn^{2+} transport channels to uniform deposition behavior on the Zn(002) crystal surface, which has been verified by grazing incidence XRD analysis. Therefore, the Zn stripping/deposition was performed in the PMC hydrogel electrolyte for 5000 h with Coulombic efficiency of 99.5%, as already evidenced in Figure 3c. Figure 6j–l shows the application of the PMC hydrogel electrolyte a Zn-ion cell using the V_2O_5 cathode. The cycle performance (Figure 6j) and related voltage profiles (Figure 6k) at a current density of 1.0 A g^{-1}, indicated that the cell can deliver a capacity ranging from 400 to 250 mAh g^{-1} over 200 charge/discharge runs, with an average working voltage of 0.9 V and a performance exceeding that of the reference aqueous electrolyte. Furthermore, the rate capability test of the battery (Figure 6l) revealed capacity higher than that of the reference solution from a current of 0.1 A g^{-1} (i.e., 400 instead of 300 mAh g^{-1}) to 2 A g^{-1} (250 instead of 190 mAh g^{-1}).[31]

Therefore, basing on these examples, we may indicate that the Zn-ion battery using the V_2O_5-type cathodes and an adequate electrolyte setup can actually represent a valid choice for energy storage, however with a voltage slope that requires a suitable tuning of the electronic setup and the battery management system to allow a proper use in the selected device.

4. Zinc–Air Rechargeable Batteries

Zn–air battery is triggering increasing interest due to its eco-sustainability and potentially high energy content. However, this intriguing battery has been hindered by several issues such as the sluggish kinetics of the air cathode, irreversible reactions at the zinc anode, and electrolyte saturation or leakage.[63] Recent articles enlightened several details regarding the geometric configuration and charge storage mechanisms in Zn–air battery, and reported insights to enhance the various constituent components of these cells.[64–66] Therefore, the academic research on rechargeable Zn–air batteries is presently growing with a considerable rate as demonstrated by the raising number of research papers.[67] The electrochemical processes in a rechargeable Zn–air battery have been described as oxygen reduction reaction (ORR) and oxygen evolution reaction (OER), and various studies have indicated that it may proceed reversibly, if allowed by the electrolyte formulation and cell setup, as below[68]

$$O_2 + 4e^- + 2H_2O \leftrightarrows 4OH^- \ (E = 0.4V \text{ vs SHE}) \quad (7)$$

Taking into account the reaction at the Zn anode, i.e.

$$Zn + 4OH^- \leftrightarrows Zn(OH)_4^{2-} + 2e^- \ (E = -1.25V \text{ vs SHE}) \quad (8)$$

followed bay equilibrium

$$Zn(OH)_4^{2-} \leftrightarrows ZnO + H_2O + 2OH^- \quad (9)$$

The overall electrochemical process becomes

$$2Zn + O_2 \leftrightarrows 2ZnO \quad (10)$$

Therefore, taking into account the potentials of anode and cathode in these conditions, the theoretical working voltage of Zn–air battery related with the overall redox process is calculated to be 1.65 V.

However, the electrolyte nature can trigger various parasitic reactions leading to the formation of a series of by-products, H_2 gas, or precipitates in particular in presence of CO_2, as reported below[68]

$$Zn + 2H_2O \rightarrow Zn(OH)_2 + H_2 \quad (11)$$

$$KOH + CO_2 \rightarrow KHCO_3 \quad (12)$$

$$2KOH + CO_2 \rightarrow K_2CO_3 + H_2O \quad (13)$$

The formation of these undesired chemicals, as well as hindered kinetics of the ORR/OER that can foresee the formation of intermediates or even different reaction mechanisms, have lowered the discharge voltage of the cell below 1.2 V, and increased the charge voltage over 2 V in practical systems at current densities ranging from 1 to 10 mA cm^{-2}. This huge polarization and the abovementioned issues so far limited the energy efficiency of the rechargeable Zn–air battery to values below 60%.[69] Therefore the proper choice of ad hoc designed and functionalized electrolyte appeared crucial to boost further the development of this important energy storage system. Lignocellulose-based gels and polymers have certainly contributed to the growth of the Zn–air battery, due to the flexibility of the derivatives and the large room for functionalization and design, as well as for their high conductivity, water uptake, and tunable electrochemical activity both at the oxygen cathode side and at the Zn metal anode one. For example, a flexible Zn–air battery has used a PANa-based gel electrolyte with GO and CNF.[50] The incorporation of rigid GO and CNF into a PANa-bonded network of the GPE significantly improved the conductivity as well as the mechanical properties. Hence, the conductivity has been measured to be 178.6 mS cm^{-1}, and the electrolyte revealed elongation capability over 14 times of its initial length, thus denoting a remarkable flexibility. Sandwich-structured flexible Zn–air battery using this gel electrolyte exhibited an extended cycle life of over 214 h at 2 mA cm^{-2}, and operated even under bending.[50] Another GO-based GPE revealed an enhanced mechanical strength and ionic conductivity, and therefore the membrane has been employed in flexible

Zn–air battery with prolonged cycling performance.[49] The gel electrolyte involved PANa incorporating GONR and CNF. This hydrogen bonds in PANa/CNF/GONR electrolyte created ionic conductive channels, enhancing the ionic conductivity and battery performance. The electrolyte demonstrated relevant water retention, stretchability up to 20 times its length, and ion conductivity of 268 mS cm^{-1}. **Figure** 7a shows the synthesis scheme of the PANa/CNF/GONR, while Figure 7b–e reveals the performances of a rechargeable Zn-air battery with this gel and reference ones based on PAN/CNF and PAN/CNF/GO. In general, the battery using PANa/CNF/GONR electrolyte showed higher performances compared to the reference ones, with a capacity for the complete discharge until 0 V at 2 mA cm^{-2} of 560 mAh g^{-1} as referred to Zn weight (Figure 7b), delivered mainly at about 1.25 V, and a power density of 90 mW cm^{-2} (from curves in Figure 7c). Furthermore, the cell using PANa/CNF/GONR electrolyte cycled galvanostatically at 2 mA cm^{-2} by limiting discharge or charge time to 10 min operated for over 320 h (i.e., 960 cycles in Figure 7d), and exhibited better response at higher current density than the reference (Figure 7e). In the same study, a cable-type all-solid-state Zn–air battery achieved an energy density of 88 mW cm^{-2} with high flexibility, indicating potentiality for wearable energy applications.[49] A further gel polymer electrolyte has been proposed for solid-state rechargeable Zn–air battery.[44] The electrolyte was synthesized by cross-linking PAA and ultrafine cellulose with the PVA to achieve the composite gel (PVAA—cellulose). The extensive porous network and hydrogen bonding of the PVAA—cellulose have led to optimal water retention, and thermal stability, with ionic conductivity of 123 mS cm^{-1}, all values higher if compared with PVAA (i.e., the mixture of PVA and PAA). The cycling performances of the PVAA—cellulose electrolyte demonstrated the inhibition of the dendrite growth and of oxidation byproduct generation, which contributed to the cycling stability of the Zn–air battery. Figure 7f shows a scheme of the PVAA—cellulose solid state electrolyte (SSE) synthetic procedure. The discharge polarization and power density curves of the Zn–air batteries revealed a better behavior of the cell using PVAA—cellulose SSE compared to the cells using PVA and PVAA, with a power density of 74 mW cm^{-2} (Figure 7g), and a lower polarization for discharge limited to 10 minutes until 10 mA cm^{-2} (Figure 7h).

Furthermore, the voltage–capacity curve in Figure 7i indicated for the cell using the PVAA—cellulose electrolyte a specific capacity of 720 mAh g^{-1} as referred to the Zn weight for the copmlete discharge until 0.5V, delivered mainly at about 1.25 V. The EIS spectra evidenced interphase resistance of the cell of few ohms (Figure 7j), and the galvanostatic discharge–charge cycling curves at 3 mA cm^{-2} by limiting charge/discharge time to 10 min revealed a stability for 54 h (i.e., 160 cycles in Figure 7k) as well as the outstanding flexibility.[44] Another recent research presented a CMC—PVA GPE for Zn–air battery.[46] The authors optimized the process to achieve the electrolyte that retained a relevant KOH amount to favor the electrochemical processes of the MnO_2-based air cathode and the Zn anode. The ratio of PVA:CMC, concentration of PVA—CMC, and thickness of the gel polymer electrolyte have been adequately tuned. The research results have shown that the gel using a polymer membrane with PVA:CMC ratio of 5:2 at a concentration of 0.063 g mL^{-1} in DI water can uptake 6 M KOH, thus lowering the charge transfer resistance (R_{CT}) of the device, and increasing the discharge plateau by 5–6 times compared to a gel using PVA only. **Figure** 8a shows the scheme of the polymer matrix, and Figure 8b reveals the notable uptake of the gel polymer electrolyte during time evolution. The cycling performance of the Zn–air battery using MnO_2 nanowires with 10 min duration limit for each discharge (5.2 mA cm^{-2}) or charge (7.3 mA cm^{-2}) reported in Figure 8c evidences a life extended over 75 cycles, average working voltage of about 1.3 V, however initial polarization of 0.66 V (Figure 8d) increasing to about 1 V at the end of the test (Figure 8e), which is justified by the increase of the cell impedance demonstrated by the EIS of the device before and after cycling (Figure 8f). It is worth mentioning that the electrolyte uptake (Figure 8g) was correlated with R_{CT} of the device. On the other hand, a Zn–air battery using the same electrolyte setup with a new porous Ni foam (air electrode) has been assembled and cycled. Figure 8h shows the discharge capacity curve of this cell from OCV (inset) down to 0 V at 1 mA cm^{-2}, and reveals a working voltage of about 1.3 V and a maximum discharge capacity of 710 mAh g^{-1} as referred to the Zn weight. Furthermore, the cycling performance of this battery (Figure 8i), within the same condition of the previous one (compare with Figure 8c) depicted a reversible trend over 310 cycles (charge/discharge limit of 10 min), thus suggesting the cathode optimization as a suitable strategy to improve the battery performance in addition to the proper electrolyte setup.[46] A further literature example has interestingly shown concomitantly CO_2-retardant effect and energy storage in a system based on CO_2-decorated conductive cellulose electrolyte.[48] The work focused on the achievement of highly conductive cellulose by bedecking the cellulose with CO_2 (CC—CO_2) via ionization, which brooked the inherent inter- and intra-molecular hydrogen bonds. The material was used as a quasisolid Zn–air battery which can impede the CO_2 poisoning of the electrolyte and dendrite formation on Zn to promote the electrochemical performance and stability even in a CO_2-rich atmosphere. Figure 8j reveals that the battery using the CC—CO_2 electrolyte can stand for 60 h (about 300 cycles), limiting to 10 min the cycle duration, with polarization slightly below 1 V and the working voltage of 1.4 V, while the cell using the CC operated in the same condition for less than 20 h (100 cycles). The paper claimed that facilely and recycling efficiency of the materials, as well as integrating CO_2 utilization with bioderived materials was well designed for renewable energy storage systems to meet sustainability targets.[48] Another biodegradable electrolyte was recently designed for flexible energy storage system in literature for lowering the cost, and increasing the safety.[47] Hence, a quaternized soybean protein isolate (QSPI) with highly hydrophilic polymer hydroxyethyl cellulose (HEC) electrolyte (QSPI@HEC) characterized by relevant ionic conductivity, up to 24 mS cm^{-1}, has been prepared and applied in a Zn–air battery. The activation energy of ion transport has been obtained for this membrane by calculating the slope of $\ln(\sigma)$ versus $(1000/T)$ according to the Arrhenius equation, and OH^- transport has been described to be principally controlled by the Grotthuss mechanism. The resulting Zn–air battery performed at various current densities exceeding the reference membrane (Fumasep FAA-3-PK-75 FAA-3-PK-75), with discharge plateau of 1.3 V at 0.5 mA cm^{-2} and 1.2 V at 10 mA cm^{-2}, at a time limited to 10 min for each current (Figure 8k), and peak power density of up to 80 mW cm^{-2}. The galvanostatic discharge–charge cycling current at 1 mA cm^{-2}

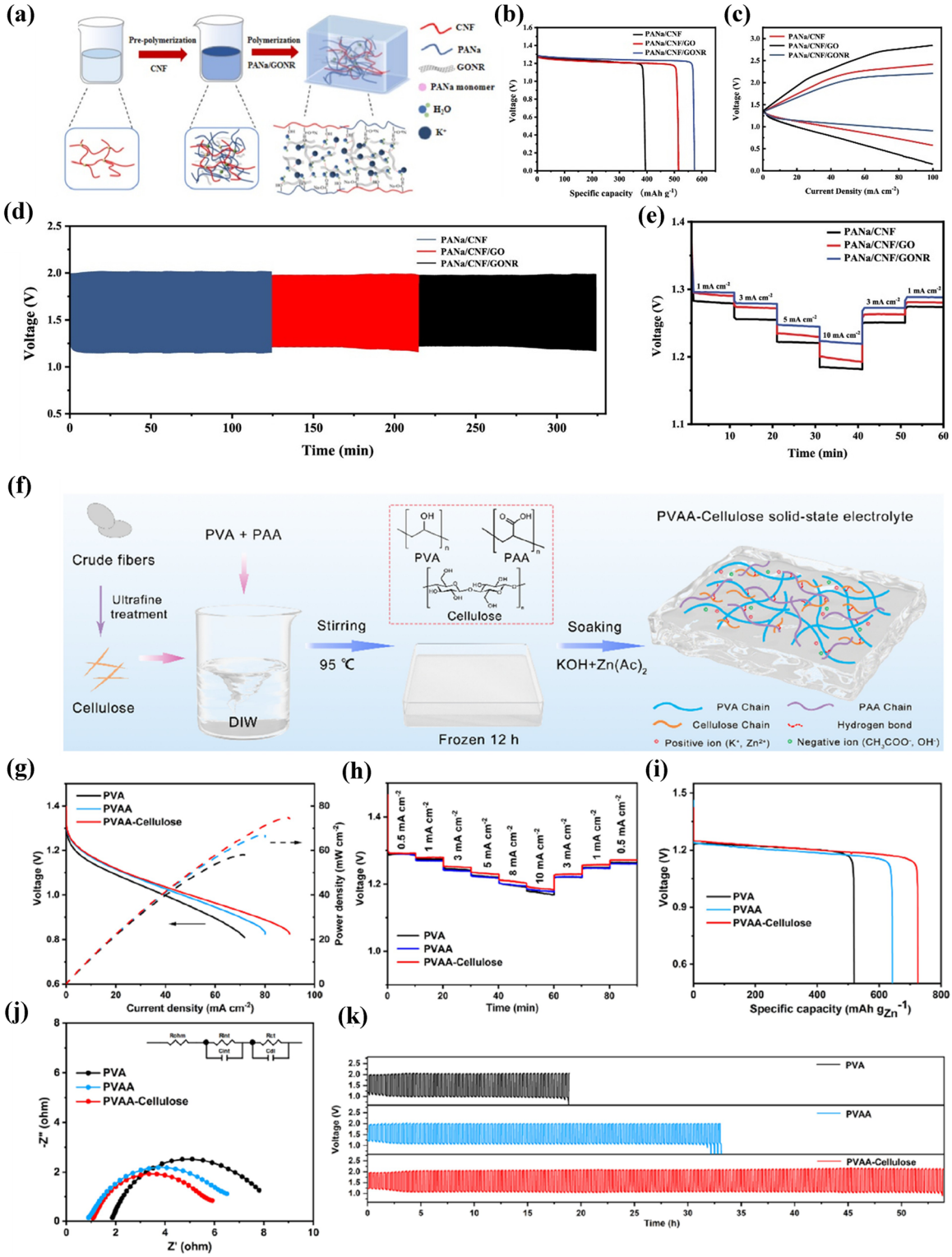

Figure 7. a–e) Characteristics of the PANa/CNF/GONR GPE. (a) Synthesis scheme, (b) discharge curves at 2 mA cm^{-2} until 0 V of Zn–air battery based on different GPEs and (c) power densities curves. (d) Galvanostatic charge–discharge cycling of the batteries based on different GPEs at 2 mA cm^{-2} limiting discharge or charge time to 10 min and (e) discharge curves at different current densities. Adapted with permission.[49] Copyright 2024, ACS. f–k) Characteristics of PVAA—cellulose SSEs. (f) Synthetic procedure scheme. (g) Discharge polarization and power density curves of Zn–air battery using PVA, PVAA, and PVAA—cellulose SSEs. (h) Discharge curves at different current densities limiting the time to 10 min. (i) Voltage–capacity discharge curves until 0.5V, (j) EIS, and (k) galvanostatic discharge–charge cycling curves at 3 mA cm^{-2} limiting discharge or charge time to 10 min. Adapted with permission.[44] Copyright 2023, ACS. See Table 1 for acronyms' summary.

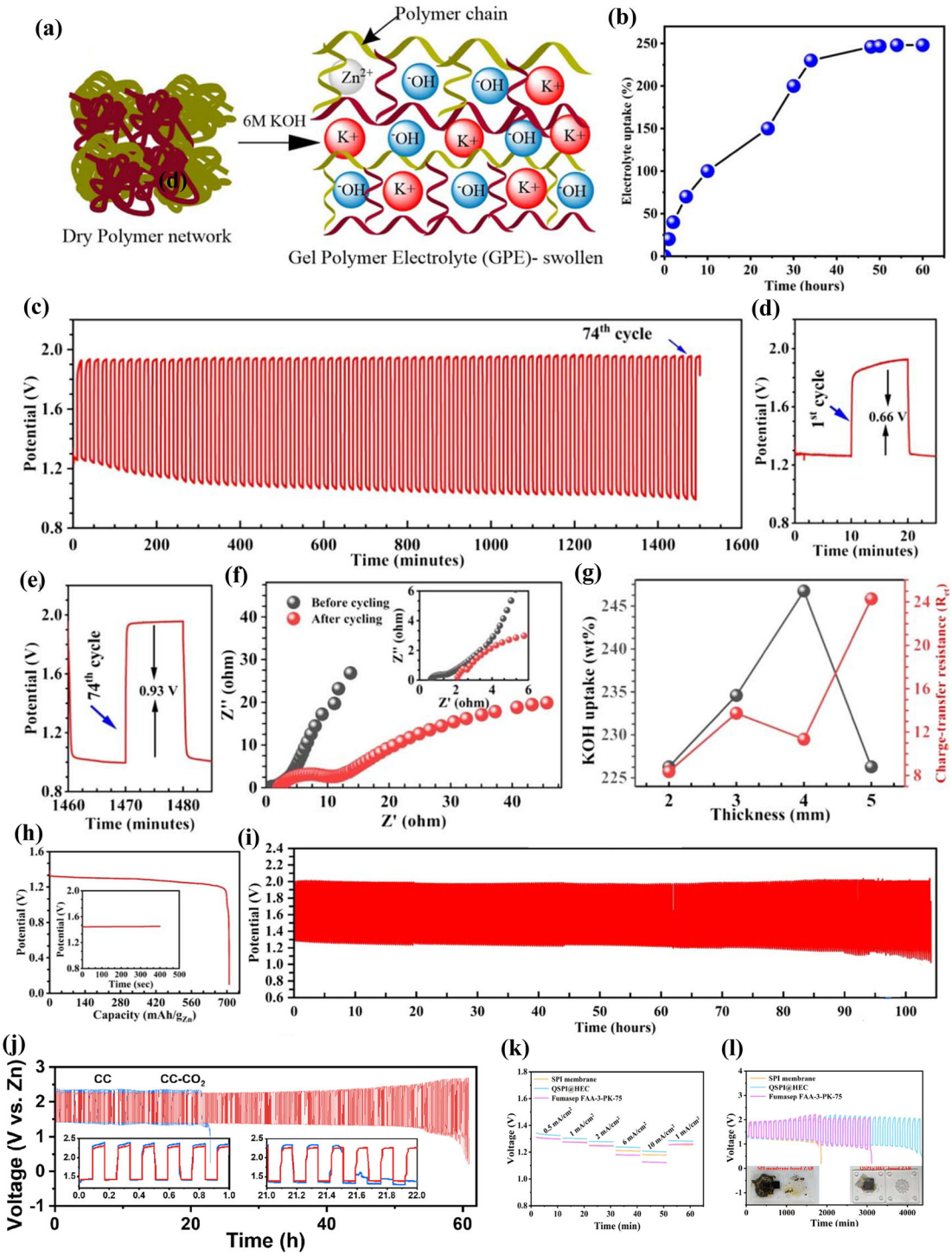

Figure 8. a–c) CMC—PVA GPE composite GPE. (a) Scheme of the polymer matrix. (b) Electrolyte solution (6 M KOH) uptake of the GPE (PVA: CMC: 5:2, thickness: 4mm) during time. (c) Cycling trend of Zn–air battery using MnO_2 nanowires by discharge at 5.2 mA cm^{-2} and charge at 7.3 mA cm^{-2} for 10 min each, with 4 mm thick GPE, d) first cycle and e) last cycle (75th). f) EIS before and after cycling, g) electrolyte uptake of each sample and correlation with R_{CT} of the device. h) Discharge capacity curve of a Zn–air battery with the same electrolyte and new porous Ni foam (air electrode) from OCV (inset) to 0 V at 1.0 mA cm^{-2}, and i) cycling performance by discharging at 5.2 mA cm^{-2} and charging at 7.3 mA cm^{-2} for 10 min each. Adapted with permission.[46] Copyright 2024, ECS. j) Cycling curves at the specific cycling time (10 min per cycle) of Zn–air batteries in air at 1 mA cm^{-2} using bare and CC—CO_2 electrolytes. Adapted with permission.[48] Copyright 2022, RSC. k) Rate capability of the solid-state Zn–air battery assembled with QSPI@HEC electrolyte and commercial reference membrane (discharge time limited to 10 min for each current), l) cycling performance of battery with the galvanostatic discharge–charge current at 1 mA cm^{-2} and a duration of 1 h per charge or discharge. Adapted with permission.[47] Copyright 2024, ACS.

with duration limited to 1 h per charge or discharge was stable for around 4300 min (36 cycles), clearly exceeding the reference samples (Figure 8l).[47]

The rechargeable Zn–air cell examples reported above demonstrated the feasibility of this technology by properly tuning the electrode/electrolyte interphase characteristics. However, the cells revealed a still persistent issues ascribed to the sluggish kinetics, which lead to acceptable cycle life only if a small fraction of the capacity is exploited (typically less than 1/10 of the one achievable by full discharge until low voltage). These drawbacks may be mitigated by the adequate cell setup, including the presence of catalysts in the cathode side. On the other hand, the best-known catalyst for OER is RuO_2, and for ORR is Pt/C, respectively, which suffer from many disadvantages, e.g., high cost, and modest stability in the electrolyte especially at the higher oxidation potential.[63,70,71] Further candidates with more sustainable cost are transition metal oxide electrocatalysts, that are widely recognized for the ability in facilitating both OER and ORR, due to their partially filled d-orbitals that facilitate numerous possible oxidation states. Additionally, performance enhancement can be achieved through doping or combining with other complementary materials like carbon-based ones.[72–75]

5. Evaluation on Energy Density, Applicability, and Future Outlooks

In the previous paragraphs, we have illustrated examples of rechargeable Zn batteries operating by using different cathode chemistries, i.e., MnO_2, V_2O_5, and air, exploiting the cellulose-based membrane as the aqueous electrolyte media. Despite there are many other examples of Zn cells with the setup discussed herein,[76–79] as well as using different electrolyte media,[80,81] it appeared to us that cellulose-based substrates are among the most convenient in terms of processability and low economic and environmental impact.[82–84] Unlike materials predominately derived from fossil feedstocks and minerals which can trigger climate change, plastic pollution, and economic challenges, cellulose represents a versatile substrate perceived by relevant stakeholders to be biodegradable, and sustainable. In addition, cellulose-based materials derived from various natural products and even from biowaste can be transformed into hydrogels, aerogels, membranes, films, and fibers by conventional and low-cost synthetic pathways, which further triggers the sustainability.[85] On the other hand, our review indicates that various problems of the mainstream cathode materials, such as MnO_2 dissolution and its possible loss in the cell or V_2O_5 deterioration, can by strongly limited by the several optimizations of the cellulose-based membrane. Hence, among the batteries illustrated above, the cell using the COP—CMC/QG—Zn and Zn/MnO_2 cathode rather than the bare electrode in Figure 4c revealed a cycle life extended over 1000 cycle with very modest decay, the cell with PIM gel membrane and the same cathode in Figure 4e retained 85% of the pristine capacity over 400 cycles, while the one using Zn–gel from cellulose/DES and carbon cloth@MnO_2 (CC@MnO_2) in Figure 5c showed 500 cycles with very limited decay. The same improvement has been observed for vanadium-oxide-based cathode with cellulose membranes, as clearly evidenced by the performance of the $NH_4V_4O_{10}$/CAZ@Zn cell in Figure 6e that depicted a life extended over 2000 cycles without any significant decay. Therefore, the use of cellulose-based membranes can substantially mitigate the still existing issues of diffused cathodes such as MnO_2 and V_2O_5. The energy content and the cycle life of the cells discussed herein differed depending on the feature of electrolyte and cathode sides. Hereafter, we compare the characteristics of the various cell prototypes with the aim of enlightening possible applicability in suitable fields according to the energy and economical requests.[86] Hence, for achieving this scope, **Table 2** reports a summary of the Zn- cell characteristics shown in the various figures of this work in terms: i) battery type; ii) working voltage considered as the average value for the sloped or multishaped curve in Zn-ion cells (i.e., the ones using MnO_2- and V_2O_5-type cathodes), while an almost constant discharge plateau of about 1.3 V for the Zn–air battery; iii) the maximum specific capacity that is typically achieved at the lowest current, normalized to the active material weight in the cathode for Zn-ion batteries, and to the Zn anode weight for the Zn–air cells; iv) the starting capacity during long-term cycling, considered as the one after the initial few stabilization runs, with related current, capacity retention, and total number of cycles. It is worth noticing that the cycle number is reported only as indication also for Zn–air cell, and it cannot be directly compared to the cycle life of the typical Zn-ion cells since it is achieved by limiting the discharge time, hence the cell capacity, to a very small fraction of the full discharge one. On the other hand, the Zn–air cells reveal the highest capacity value upon a single discharge without limitation, which is however not fully reversible, instead the cells using MnO_2 have the highest working voltage value despite the lowest maximum capacity, and they share with cells using V_2O_5-type cathode the most relevant cycle life within a practical condition comparable to that of other rechargeable systems. Despite of the lowest average working voltage among the other cells, the ones using V_2O_5 cathode remark a relevant competitivity in terms of high capacity value and feasibility.

Therefore, we may suggest that the Zn-ion batteries are presently the most competing in terms of gravimetric capacity and cycle life, while the Zn–air one is still the most promising, while requesting further development to achieve at the same time high capacity and long cycle life. A further insight to facilitate the comparison is reported in **Figure 9** that summarizes the performances in term of expected energy density of the various cells discussed herein. It is worth mentioning that the expected energy density has been calculated taking into account the maximum capacity of the cell and its average working voltage, as well as a reduction factor to take into account the contribution of inactive elements, such as the cell case, current collectors, and cell body components. This reduction factor has been considered 1/3 for the Zn-ion cells, which is a conventional fraction typically used in the case of the most diffused rechargeable batteries, such as the Li-ion ones.[87] On the other hand, the reduction factor is lowered to 1/10 for the Zn–air cells, that employ gas diffusion layers, foams, and other materials to allow the oxygen diffusion, and foresee the limitation of the maximum capacity to a small fraction by tuning the charge/discharge time for rechargeability. It is worth mentioning that such a drastic normalization is typically performed also for the Li–oxygen (Li–air) rechargeable batteries that share very similar issues.[88,89] Interestingly, the figure evidences that the practical energy density ranged from a maximum of 135 Wh kg^{-1} for the most performing cell to 75 Wh

Table 2. Characteristics of the various rechargeable Zn-batteries reported in this review in terms of average working voltage, gravimetric specific capacity, and cycle life.

Refs. *n*/Figure *n*	Battery	Voltage [V]	Maximum capacity [mAh g^{-1}]	Long-tern cycling initial capacity [mAh g^{-1}]	Long-tern cycling capacity retention [%]	Long-tern cycling employed current [A g^{-1}]	Provided cycles
[40]/Figure 4	Zn–MnO_2	1.35	300[a)]	150	80	1	1000
[34]/Figure 4	Zn–MnO_2	1.35	220[a)]	120	91	0.15	400
[43]/Figure 4	Zn–MnO_2	1.35	140[a)]	140	77	0.1	100
[36]/Figure 5	Zn–MnO_2	1.35	210[a)]	200	90	0.15	500
[33]/Figure 5	Zn–MnO_2	1.35	225[a)]	130	54	1	500
[32]/Figure 6	Zn–$NH_4V_4O_{10}$	0.8	420[a)]	175	97	1	2000
[41]/Figure 6	Zn–V_2O_5	0.8	420[a)]	400	63	0.1	200
[31]/Figure 6	Zn–V_2O_5	0.8	410[a)]	390	71	1	500
[49]/Figure 7	Zn–Air	1.25	560[b)]	–	–	–	960[c)]
[44]/Figure 7	Zn–Air	1.25	720[b)]	–	–	–	160[c)]
[46]/Figure 8	Zn–Air	1.3	710[b)]	–	–	–	310[c)]
[48]/Figure 8	Zn–Air	1.3	780[b)]	–	–	–	350[c)]
[47]/Figure 8	Zn–Air	1.4	600[b)]	–	–	–	36[c)]

[a)] Calculated taking into account the cathode active material weight; [b)] Calculated taking into account the Zn anode weight; [c)] Achieved by limiting the discharge time to a small fraction of the full discharge (below 10% of the maximum value for full cell discharge).

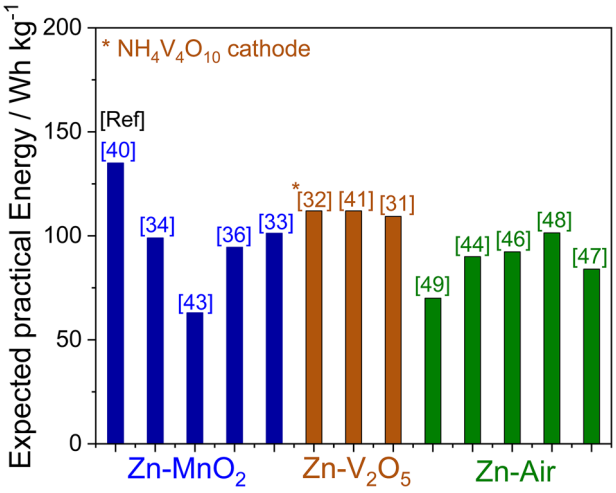

Figure 9. Expected practical gravimetric energy density values of the various cells discussed herein, divided by 3 families: Zn–MnO_2, Zn–V_2O_5, and Zn–air.

kg^{-1} for the less performing ones.[44] In detail, one example of Zn–MnO_2 cell revealed a very promising value (135 Wh kg^{-1})[40] which is almost competing with the one of the Na-ion cells,[90] with the additional bonuses of the relevant applicability and the long cycle life in practical battery (see Table 2 for details). Relevantly, all cells using V_2O_5-type electrode show a similar competing value of around 110 Wh kg^{-1},[31,32,41] while the rechargeable Zn–air cells show a maximum value of bout110 Wh kg^{-1} and the advantage of wearability for possible niche applications.[48] The data reported in Figure 9 show for all the rechargeable Zn cells an energy value which is typically well accepted for applications in stationary storage, which is more affected by the battery cost than weight and volume, rather than electric vehicles field.[86] However, we would mention that the future development of rechargeable batteries based on Zn and cathodes such as MnO_2, V_2O_5, or oxygen requires the ultimate solution of problems such as metal dissolution, cathode deactivation, or dendrite formation at the anode side. Despite this review evidenced that several improvement have been already made, the actual large-scale diffusion of these rechargeable systems may be achieved by further optimizing all the cell components. In particular, Zn anode may be enhanced by using coatings, alloying systems, or direct electroplating in a Zn-metal-free version. The cathodes can be additionally modified by coating, doping, or by building 3D structures, preintercalation of guest species, introduction of defects, or by optimizing nanostructures. The electrolyte can be optimized by using ad hoc additives or separators, improving the strength, functionalization of flexible gel or plasticized membranes, and selecting proper Zn salts.[52,57] In particular, synergistic interaction between all the three components is considered the pathway of choice, in particular for Zn–air battery which is the most challenging system.[67]

Among the recent electrolyte optimizations, we can mention that membranes with asymmetrical proton transport for cross-communication harmony have been used as extreme lean electrolyte for Zn–vanadium battery,[91] whilst MXene-cellulose nanofibril ionotronic dual-network hydrogel films were successfully employed to stabilize the zinc anodes.[92] Furthermore, nanocellulose-carboxymethylcellulose electrolyte has been developed ad hoc for Zn-ion batteries characterized by excellent stability and high-rate,[93] and ultrathin cellulosic gel electrolytes with a gradient hydropenic interface have been adopted for developing stable, high-energy and flexible Zn-battery.[94] On the other hand, nanoengineered functional cellulose has been developed as ionic conductor for achieving all-solid-state Zn-ion battery with relevant performance,[95] and CNCs have been built to achieve multiscale hydrogel electrolyte used in highly reversible and flexible Zn-ion battery.[96] An ultrastable Zn anode has been achieved using amphoteric cellulose-based double-network hydrogel,[97] whereas electrolytes with abundant ion and water channels have been derived from biomass for solid-state and flexible Zn–air battery.[98] As an ultimate proof of the system applicability,

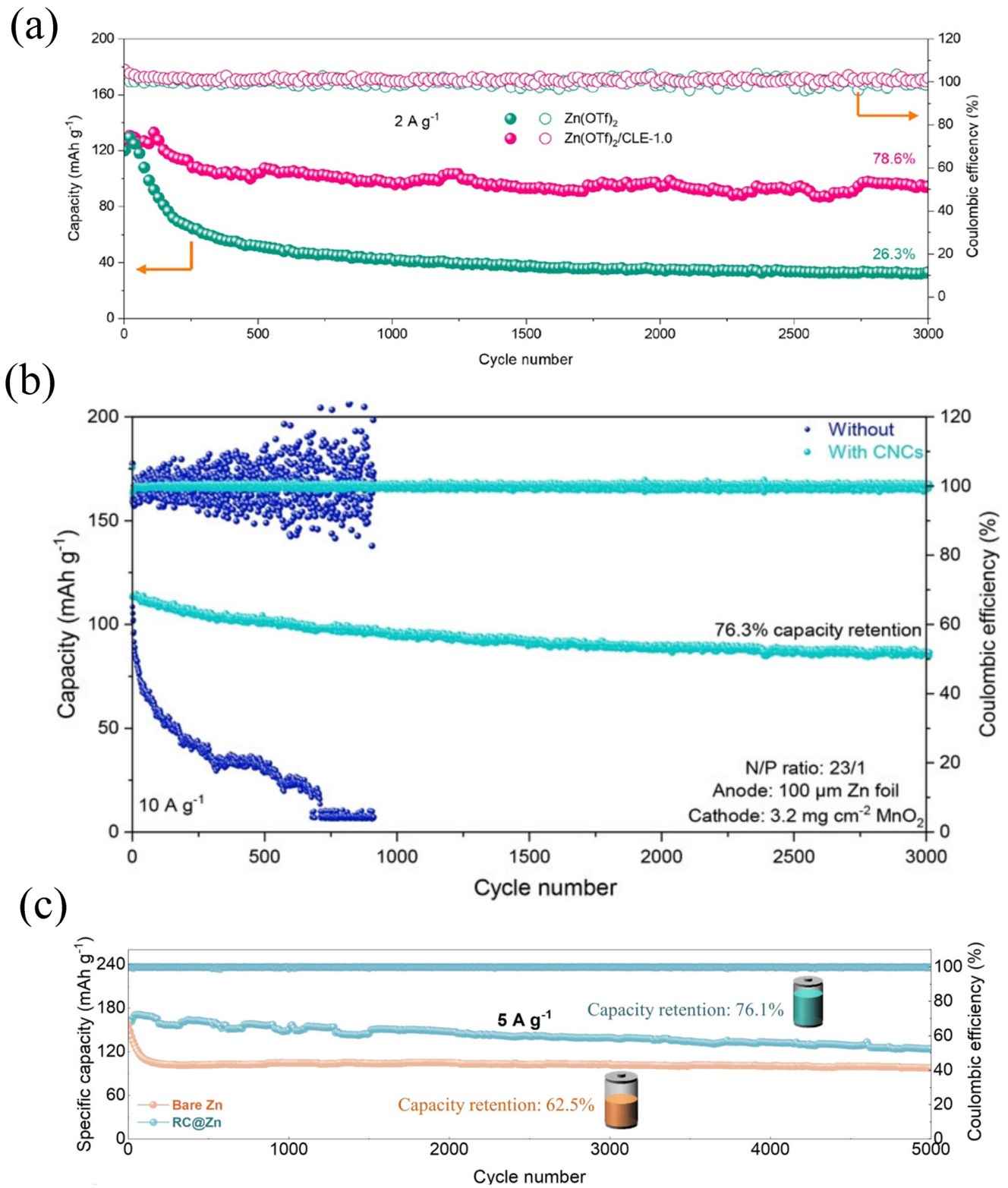

Figure 10. Zn-ion cells with relevantly improved cycling performance. a) Zn–MnO_2 cell with biobased multifunctional cellulose levulinate ester in the electrolyte cycled at 2 A g^{-1}. Adapted with permission.[99] Copyright 2024, Elsevier. b) Zn–MnO_2 cell with multifunctional CNC in the electrolyte cycled at 10 A g^{-1}. Adapted with permission.[100] Copyright 2024, Wiley. c) Zn–V_2O_5 cell with molecular chain rearrangement of natural-cellulose-based artificial interphase cycled at 5 A g^{-1}. Adapted with permission.[101] Copyright 2025, Wiley.

Figure 10 reports some of the most improved Zn-ion batteries recently reported in literature.

Impressively, biobased multifunctional cellulose levulinate ester,[99] and multifunctional CNC[100] have been used as the electrolyte additive for getting Zn–MnO_2 battery with cycle life extended over 3000 cycles (Figure 10a,b, respectively). Equally impressive appeared the 5000 stable cycles of the Zn–V_2O_5 battery exploiting molecular chain rearrangement of natural-cellulose-based artificial interphase on the Zn metal anodes (Figure 10c),[101] whereas molecule-adsorption-induced interface served as a regulator for Zn–MnO_2 battery with relevant cycle life.[102]

6. Remarks and Conclusions

This review reported a series of rechargeable Zn- batteries based on lignocellulose polymers and hydrogels, categorized by taking into account the cathode side, i.e., manganese oxide, vanadium oxide, and air, all proposed as energy storage systems for lowering the costs and enhancing the environmental sustainability. The work revealed substantial tunability of the membrane synthesis techniques, that allowed the preparation of various types of functionalized electrolytes, characterized by compatibility both with Zn anode and with the cathode side. Thanks to functional groups such as —OH, —NH_2, —COO, and —CO, these membranes allowed adequate hosting of the Zn^{2+} ions in the backbone, and at the same time high conductivity exceeding 1×10^{-3} mS cm^{-1}, low Zn–electrolyte interphase resistance, and suppressed dendrite formation. For example, COP—CMC/QG has foreseen a hydrophilic multifunctional layer in which carboxyl and hydroxyl or ether groups intimately contacted the Zn metal and the Zn^+ ion conducting media. This setup actually allowed Zn–MnO_2 rechargeable battery with promoted kinetics and cycle life. On the other hand, additional groups such as the amidoxime in the AO-PIM-1/BC GPE showed a synergic effect between the abovementioned groups and the C═N bonds that coordinated Zn^{2+} to further promote the ion transport, reduce the desolvation energy, and allow uniform deposition of Zn, thus triggering the electrolyte performances. Hence, we can reasonably conclude that the concomitant effect of coordinating functional groups such as carboxyl, hydroxyl, ethers, and other additional groups such as —CN or —SO, are the main responsible for the improvement of the cellulose-based electrolyte membranes in terms of Zn-transference number, ion conductivity, cell stability, kinetics, and cycle life. In addition, various membrane prototypes resulted elastic and with notable mechanical strength, thus allowing possible scalability of the system. Regarding the Zn- cell performances, the study revealed the possible achievement of long cycling life, in particular for the batteries using the MnO_2 and V_2O_5 cathodes. In detail, projections on the achievable practical energy have indicated for a Zn–MnO_2 cell a value of 135 Wh kg^{-1}, which competed with the one of Na-ion battery, while all the Zn–V_2O_5-type cells steadily evidenced an energy of about 110 Wh kg^{-1}. On the other hand, the Zn–air cells showed promising performances with the maximum energy density of 100 Wh kg^{-1}, which can be further improved. Indeed, these cells delivered the maximum discharge capacity, the reversibility of which was still hindered by sluggish kinetics of the process leading to relevant polarization and possible cell failure, unless capacity limitation to a fraction of the maximum value is adopted to increase the lifespan. Furthermore, the cells using the V_2O_5 cathode evidenced the widest voltage slope during operation, i.e., extending from 0.3 to 1.5 V, instead the ones using MnO_2 operated between 1 and 1.5 V, and the Zn–air system discharged at constant voltage of 1.3 V however with the abovementioned capacity limitation and polarization. Therefore, we may conclude that all these cells may be adequate candidates for energy storage, while the Zn–MnO_2 ones appeared the most advanced example for possible scalability. Furthermore, recent and relevant progresses on the cellulose-based electrolytes have actually led to impressive performance in terms of cycle life and stability of Zn-ion batteries using MnO_2 and V_2O_5 cathodes, thus suggesting a concrete possibility for future practical application of these energy storage systems. Indeed, Zn–MnO_2 using biobased multifunctional cellulose levulinate ester,[99] and multifunctional cellulose nanocrystals[100] revealed lifespan extended over 3000 cycles, while Zn–V_2O_5 battery exploiting molecular chain rearrangement of natural-cellulose-based artificial interphase delivered 5000 stable cycles.[101] Additional insight may be given by considering that these batteries cannot compete with Li-ion ones in terms of energy density, which is the most challenging request of electric vehicles.[103–105] Rather, these sustainable systems can actually serve as the power supply for employment in gird stabilization and stationary energy storage from discontinuous, while notably green and renewable sources, such as solar, wind, and geothermal.[106–108] These systems are in fact more affected by cost than energy density, and are requested for limiting fossil-fuel energy production and decreasing the greenhouse gas emission that may trigger global warming.[109,110] On the other hand, a possible decrease of the vehicle weight by using new composite materials, such as carbon fibers,[111,112] can even open a room for using the rechargeable Zn-based battery in electrified road transportation, thus further limiting emission from combustion engine technology.[113,114]

Acknowledgements

This work was supported by the Institute of Global Innovation Research (GIR) in Tokyo University of Agriculture and Technology, Japan, and by the Fondo di Ateneo per la Ricerca Scientifica (FAR 2024) University of Ferrara, Italy.

Open access publishing facilitated by Universita degli Studi di Ferrara, as part of the Wiley - CRUI-CARE agreement.

Conflict of Interest

The authors declare no conflict of interest.

Keywords

air, cellulose electrolyte, manganese oxide, vanadium oxide, zinc

Received: March 10, 2025
Revised: May 12, 2025
Published online: June 8, 2025

[1] L. Lu, X. Han, J. Li, J. Hua, M. Ouyang, *J. Power Sources* **2013**, *226*, 272.
[2] T. Chen, Y. Jin, H. Lv, A. Yang, M. Liu, B. Chen, Y. Xie, Q. Chen, *Trans. Tianjin Univ.* **2020**, *26*, 208.
[3] D. Di Lecce, V. Marangon, H.-G. Jung, Y. Tominaga, S. Greenbaum, J. Hassoun, *Green Chem.* **2022**, *24*, 1021.
[4] B. Scrosati, J. Hassoun, Y.-K. Sun, *Energy Environ. Sci.* **2011**, *4*, 3287.
[5] H. D. Yoo, E. Markevich, G. Salitra, D. Sharon, D. Aurbach, *Mater. Today* **2014**, *17*, 110.
[6] A. Manthiram, Y. Fu, Y. S. Su, *Acc. Chem. Res.* **2013**, *46*, 1125.
[7] A. Patil, V. Patil, D. W Shin, J.-W. Choi, D.-S. Paik, S.-J. Yoon, *Mater. Res. Bull.* **2008**, *43*, 1913.
[8] W. Schlemmer, J. Selinger, M. A. Hobisch, S. Spirk, *Carbohydr. Polym.* **2021**, *265*, 118063.
[9] Z. Yhobu, A. Siddiqa, M. Padaki, S. Budagumpi, D. H. Nagaraju, *Energy Fuels* **2022**, *36*, 14625.
[10] M. Zhang, Y. Duan, T. Chen, J. Qi, T. Xu, H. Du, C. Si, *Ind. Crops Prod.* **2023**, *203*, 117174.
[11] M. Song, H. Tan, D. Chao, H. J. Fan, *Adv. Funct. Mater.* **2018**, *28*, 1802564.
[12] L. E. Blanc, D. Kundu, L. F. Nazar, *Joule* **2020**, *4*, 771.
[13] J. Shin, J. W. Choi, *Adv. Energy Mater.* **2020**, *10*, 2001386.
[14] K. Kordesch, W. Taucher-Mautner, in *Encyclopedia of Electrochemical Power Sources*, Elsevier, Amsterdam, Netherlands **2009**, pp. 43–54.
[15] J. Ming, J. Guo, C. Xia, W. Wang, H. N. Alshareef, *Mater. Sci. Eng., R* **2019**, *135*, 58.
[16] W. Liu, X. Zhang, Y. Huang, B. Jiang, Z. Chang, C. Xu, F. Kang, *J. Energy Chem.* **2021**, *56*, 365.
[17] Z. Wang, H. Li, Z. Tang, Z. Liu, Z. Ruan, L. Ma, Q. Yang, D. Wang, C. Zhi, *Adv. Funct. Mater.* **2018**, *28*, 1804560.
[18] K. Lu, T. Jiang, H. Hu, M. Wu, *Front. Chem.* **2020**, *8*, 546728.
[19] Y. Tian, S. Chen, S. Ding, Q. Chen, J. Zhang, *Chem. Sci.* **2023**, *14*, 331.
[20] Y. Tian, G. Zeng, A. Rutt, T. Shi, H. Kim, J. Wang, J. Koettgen, Y. Sun, B. Ouyang, T. Chen, Z. Lun, Z. Rong, K. Persson, G. Ceder, *Chem. Rev.* **2021**, *121*, 1623.
[21] G. L. Soloveichik, *Annu. Rev. Chem. Biomol. Eng.* **2011**, *2*, 503.
[22] J. Montero, P. Navalpotro, A. DÉpifanio, B. Mecheri, S. Licoccia, J. Carretero-González, *J. Electroanal. Chem.* **2021**, *895*, 115442.
[23] V. Cyriac, N. Ismayil, I. S. B. M. Noor, Z. E. Rojudi, Y. N. Sudhakar, C. Chavan, R. F. Bhajantri, M. S. Murari, *Int. J. Energy Res.* **2022**, *46*, 22845.
[24] N. A. M. Noor, M. I. N. Isa, *Int. J. Hydrogen Energy* **2019**, *44*, 8298.
[25] N. E. Offia-Kalu, S. C. Nwanonenyi, B. Abdulhakeem, N. Y. Dzade, P. A. Onwalu, *J. Mol. Graphics Modell.* **2024**, *127*, 108667.
[26] X. Yin, J. Feng, Y. Chen, J. Zhang, F. Wu, W. Liu, W. Shi, X. Cao, *J. Solid State Electrochem.* **2023**, *27*, 1329.
[27] K. Rybacki, S. A. Love, B. Blessing, A. Morales, E. McDermott, K. Cai, X. Hu, D. Salas-de la Cruz, *ACS Mater. Au* **2022**, *2*, 21.
[28] C. P. Singh, P. K. Shukla, S. Singh, S. L. Agrawal, A. Srivastava, N. Asthana, A. K. Mishra, *J. Appl. Polym. Sci.* **2025**, *142*, 56702.
[29] S. Atifi, C. Miao, M.-N. Mirvakili, W. Y. Hamad, *Colloids Surf., A* **2024**, *686*, 133322.
[30] K. Jayalakshmi, Ismayil, S. H, V. Ravindrachary, G. Sanjeev, N. Mazumdar, K. M. Sindhoora, S. P. Masti, M. S. Murari, *J. Phys. Chem. Solids* **2023**, *173*, 111119.
[31] P. Lin, J. Cong, J. Li, M. Zhang, P. Lai, J. Zeng, Y. Yang, J. Zhao, *Energy Storage Mater.* **2022**, *49*, 172.
[32] X. Liu, Q. Han, Q. Ma, Y. Wang, C. Liu, *Small* **2022**, *18*, 2203327.
[33] Y. Yang, L. Shi, Y. Wu, Z. Chen, X. Zhu, L. Du, Y. Wang, *Chem. Eng. J.* **2024**, *484*, 149780.
[34] Z. Wang, Y. Wang, H. Zou, Y. Ni, X. Chen, H. Guo, F. Li, *Chem. Eng. J.* **2024**, *497*, 155540.
[35] B. Bhuvaneswari, M. Sivabharathy, L. G. Prasad, S. Selvasekarapandian, *Ionics* **2022**, *28*, 3865.
[36] Z. Zheng, W. Cheng, G. Jiang, X. Li, J. Sun, Y. Zhu, D. Zhao, H. Yu, *Small Struct.* **2024**, *5*, 2400180.
[37] I. Dueramae, M. Okhawilai, P. Kasemsiri, H. Uyama, R. Kita, *Sci. Rep.* **2020**, *10*, 12587.
[38] L. Yang, Y. Fu, H. Liu, Q. Nie, M. Zhang, Z. Shen, *ACS Sustainable Chem. Eng.* **2023**, *11*, 10311.
[39] P. Flouda, D. Bukharina, K. J. Pierce, A. V. Stryutsky, V. V. Shevchenko, V. V. Tsukruk, *ACS Appl. Mater. Interfaces* **2022**, *14*, 27028.
[40] J. Ding, Y. Liu, S. Huang, X. Wang, J. Yang, L. Wang, M. Xue, X. Zhang, J. Chen, *ACS Appl. Mater. Interfaces* **2021**, *13*, 29746.
[41] Z. Zheng, S. Yan, Y. Zhang, X. Zhang, J. Zhou, J. Ye, Y. Zhu, *Chem. Eng. J.* **2023**, *475*, 146314.
[42] W. G. Lee, D. H. Kim, W. C. Jeon, S. K. Kwak, S. J. Kang, S. W. Kang, *Sci. Rep.* **2017**, *7*, 1287.
[43] K. Kimura, V. Marangon, T. Fukuda, M. Suzuki, N. Soontornnon, Y. Tominaga, J. Hassoun, *Chem. Commun.* **2024**, *60*, 13698.
[44] W. Li, Y. Wang, R. Liu, W. Chen, H. Zhang, Z. Zhang, *ACS Sustainable Chem. Eng.* **2023**, *11*, 3732.
[45] E. García-Gaitán, D. Frattini, I. Ruiz de Larramendi, M. Martínez-Ibáñez, D. González, M. Armand, N. Ortiz-Vitoriano, *Batteries Supercaps* **2023**, *6*, 202200570.
[46] D. Choudhary, R. Bala, R. Dhiman, *J. Electrochem. Soc.* **2024**, *171*, 070533.
[47] M. Li, T. Xu, L. Huang, Z. Hu, C. Zhou, D. Li, J. Zhang, E. Hu, Z. Chen, *ACS Sustainable Chem. Eng.* **2024**, *12*, 17147.
[48] Q. Liu, X. Ou, L. Li, X. Wang, J. Wen, Y. Zhou, F. Yan, *J. Mater. Chem. A* **2022**, *10*, 12235.
[49] W. Liu, X. Zhao, X. Ye, X. Zheng, Y. Zhang, M. Wang, X. Lin, B. Liu, L. Han, Y. Ning, K. Rui, H. Li, Y. Lu, *Energy Fuels* **2024**, *38*, 6508.
[50] W. Liu, Y. Zhang, X. Zheng, M. Wang, X. Ye, B. Liu, L. Han, Y. Ning, Y. Lu, S. Zhang, H. Li, X. Zhao, *Energy Fuels* **2023**, *37*, 16097.
[51] Y. Mao, H. Ren, J. Zhang, T. Luo, N. Liu, B. Wang, S. Le, N. Zhang, *Electrochim. Acta* **2021**, *393*, 139094.
[52] L. Meng, Y. Zhu, Y. Lu, T. Liang, L. Zhou, J. Fan, Y. Kuo, P. Guan, T. Wan, L. Hu, D. Chu, *ChemElectroChem* **2024**, *11*, 202300495.
[53] N. Zhang, F. Cheng, J. Liu, L. Wang, X. Long, X. Liu, F. Li, J. Chen, *Nat. Commun.* **2017**, *8*, 405.
[54] S. Islam, M. H. Alfaruqi, V. Mathew, J. Song, S. Kim, S. Kim, J. Jo, J. P. Baboo, D. T. Pham, D. Y. Putro, Y.-K. Sun, J. Kim, *J. Mater. Chem. A* **2017**, *5*, 23299.
[55] M. Winter, R. J. Brodd, *Chem. Rev.* **2004**, *104*, 4245.
[56] Y. Zhou, F. Chen, H. Arandiyan, P. Guan, Y. Liu, Y. Wang, C. Zhao, D. Wang, D. Chu, *J. Energy Chem.* **2021**, *57*, 516.
[57] T. Zhou, L. Xie, Q. Han, X. Qiu, Y. Xiao, X. Yang, X. Liu, S. Yang, L. Zhu, X. Cao, *Coord. Chem. Rev.* **2024**, *498*, 215461.
[58] Y. Zhang, E. H. Ang, K. N. Dinh, K. Rui, H. Lin, J. Zhu, Q. Yan, *Mater. Chem. Front.* **2021**, *5*, 744.
[59] D. Kundu, B. D. Adams, V. Duffort, S. H. Vajargah, L. F. Nazar, *Nat. Energy* **2016**, *1*, 16119.
[60] Y. Yang, Y. Tang, S. Liang, Z. Wu, G. Fang, X. Cao, C. Wang, T. Lin, A. Pan, J. Zhou, *Nano Energy* **2019**, *61*, 617.
[61] P. Gao, Q. Ru, H. Yan, S. Cheng, Y. Liu, X. Hou, L. Wei, F. Chi-Chung Ling, *ChemElectroChem* **2020**, *7*, 283.
[62] D. Pan, T. Liu, Y. Zhang, H. Liu, M. Ding, L. Chen, *J. Taiwan Inst. Chem. Eng.* **2021**, *127*, 276.
[63] F. Cheng, J. Chen, *Chem. Soc. Rev.* **2012**, *41*, 2172.
[64] Y. Li, H. Dai, *Chem. Soc. Rev.* **2014**, *43*, 5257.
[65] X. Cai, L. Lai, J. Lin, Z. Shen, *Mater. Horiz.* **2017**, *4*, 945.
[66] J. Pan, Y. Y. Xu, H. Yang, Z. Dong, H. Liu, B. Y. Xia, *Adv. Sci.* **2018**, *5*, 1700691.
[67] A. Singh, R. Sharma, A. Gautam, B. Kumar, S. Mittal, A. Halder, *Catal. Today* **2025**, *445*, 115108.

[68] X. Yan, Y. Ha, R. Wu, *Small Methods* **2021**, *5*, 2000827.
[69] Q. Liu, L. Wang, H. Fu, *J. Mater. Chem. A* **2023**, *11*, 4400.
[70] R. Cao, J. Lee, M. Liu, J. Cho, *Adv. Energy Mater.* **2012**, *2*, 816.
[71] V. Caramia, B. Bozzini, *Mater. Renewable Sustainable Energy* **2014**, *3*, 28.
[72] A. Mathur, A. Halder, *Catal. Sci. Technol.* **2019**, *9*, 1245.
[73] A. Mathur, S. Kumari, A. Singh, R. Mitra, R. Sharma, K. Biswas, A. Halder, *J. Energy Storage* **2023**, *74*, 109350.
[74] J. Suntivich, K. J. May, H. A. Gasteiger, J. B. Goodenough, Y. Shao-Horn, *Science* **2011**, *334*, 1383.
[75] C. Wei, Z. Feng, G. G. Scherer, J. Barber, Y. Shao-Horn, Z. J. Xu, *Adv. Mater.* **2017**, *29*, 1606800.
[76] I. Dueramae, M. Okhawilai, P. Kasemsiri, H. Uyama, *Sci. Rep.* **2021**, *11*, 13268.
[77] H. Li, S. Askari, A. Kulachenko, M. Ek, O. Sevastyanova, *Int. J. Biol. Macromol.* **2025**, *290*, 138711.
[78] H. Zhang, X. An, Y. Yang, Y. Long, S. Nie, L. Liu, G. Yang, Z. Tian, H. Cao, Z. Cheng, H. Liu, Y. Ni, *EcoMat* **2023**, *5*, 12317.
[79] I. Ropio, A. C. Baptista, J. P. Nobre, J. Correia, F. Belo, S. Taborda, B. M. Morais Faustino, J. P. Borges, A. Kovalenko, I. Ferreira, *Org. Electron.* **2018**, *62*, 530.
[80] W. Wang, V. S. Kale, Z. Cao, S. Kandambeth, W. Zhang, J. Ming, P. T. Parvatkar, E. Abou-Hamad, O. Shekhah, L. Cavallo, M. Eddaoudi, H. N. Alshareef, *ACS Energy Lett.* **2020**, *5*, 2256.
[81] J. Guo, J. Ming, Y. Lei, W. Zhang, C. Xia, Y. Cui, H. N. Alshareef, *ACS Energy Lett.* **2019**, *4*, 2776.
[82] K. Wu, S. Zhan, W. Liu, X. Liu, F. Ning, Y. Liu, J. Zhang, J. Yi, *ACS Appl. Mater. Interfaces* **2023**, *15*, 6839.
[83] Y. Quan, H. Ma, M. Chen, W. Zhou, Q. Tian, X. Han, J. Chen, *ACS Appl. Mater. Interfaces* **2023**, *15*, 44974.
[84] K. Abe, H. Yano, *Cellulose* **2012**, *19*, 1907.
[85] X. Chen, L. Zhang, M. Zheng, C. Park, X. Wang, C. Ke, *Carbon* **2015**, *82*, 214.
[86] A. A. Kebede, T. Coosemans, M. Messagie, T. Jemal, H. A. Behabtu, J. Van Mierlo, M. Berecibar, *J. Energy Storage* **2021**, *40*, 102748.
[87] D. Di Lecce, R. Verrelli, J. Hassoun, *Green Chem.* **2017**, *19*, 3442.
[88] J.-B. Park, J. Hassoun, H.-G. Jung, H.-S. Kim, C. S. Yoon, I.-H. Oh, B. Scrosati, Y.-K. Sun, *Nano Lett.* **2013**, *13*, 2971.
[89] H. G. Jung, J. Hassoun, J. B. Park, Y. K. Sun, B. Scrosati, *Nat. Chem.* **2012**, *4*, 579.
[90] E. Goikolea, V. Palomares, S. Wang, I. R. de Larramendi, X. Guo, G. Wang, T. Rojo, *Adv. Energy Mater.* **2020**, *10*, 2002055.
[91] C. Liu, B. Lin, Z. Li, C. Liu, Y. Wang, W. Chen, W. Xu, M.-C. Li, S. Hong, L. Zhang, P. Yang, M. Wang, K. Zhao, C. Mei, *ACS Energy Lett.* **2025**, *10*, 1795.
[92] M. Liu, L. Zhang, J. Rostami, T. Zhang, K. Matthews, S. Chen, W. Fan, Y. Zhu, J. Chen, M. Huang, J. Wu, H. Wang, M. M. Hamedi, F. Xu, W. Tian, L. Wågberg, Y. Gogotsi, *ACS Nano* **2025**, *19*, 13399.
[93] L. Xu, T. Meng, X. Zheng, T. Li, A. H. Brozena, Y. Mao, Q. Zhang, B. C. Clifford, J. Rao, L. Hu, *Adv. Funct. Mater.* **2023**, *33*, 2302098.
[94] J. Zhai, W. Zhao, L. Wang, J. Shuai, R. Chen, W. Ge, Y. Zong, G. He, X. Wang, *Energy Environ. Sci.* **2025**, *18*, 4241.
[95] W. Tu, S. Liang, L. Song, X. Wang, G. Ji, J. Xu, *Adv. Funct. Mater.* **2024**, *34*, 2316137.
[96] Y. Li, S. Yang, Y. You, Y. Li, Y. Zhang, Q. Wu, S. Li, Q. Xu, J. Huang, H. Xie, *Chem. Eng. J.* **2024**, *496*, 154357.
[97] H. Zhang, X. Gan, Z. Song, J. Zhou, *Angew. Chem.* **2023**, *135*, 202217833.
[98] H. Dou, M. Xu, Z. Zhang, D. Luo, A. Yu, Z. Chen, *Adv. Mater.* **2024**, *36*, 2401858.
[99] K. Chen, Y. Chen, Y. Xu, M. Xu, Y. Li, S. Yang, Q. Wu, Q. Xu, H. Xie, J. Huang, *Energy Storage Mater.* **2024**, *71*, 103597.
[100] Q. Wu, J. Huang, J. Zhang, S. Yang, Y. Li, F. Luo, Y. You, Y. Li, H. Xie, Y. Chen, *Angew. Chem., Int. Ed.* **2024**, *63*, 202319051.
[101] J. Wang, L. Jiao, C. Yi, H. Bai, Q. Liu, Y. Fu, J. Liu, C. Wang, Y. Lei, T. Zhang, J. Wen, L. Yang, D. Shu, S. Yang, C. Li, H. Li, W. Zhang, B. Cheng, *Angew. Chem., Int. Ed.* **2025**, *64*, 202418992.
[102] J. Zhang, X. Wei, Q. Wu, X. Liu, S. Yang, F. Luo, Z. Yan, J. Huang, Y. Chen, *Polym. Sci. Technol.* **2025**, https://doi.org/10.1021/polymscitech.4c00034.
[103] H. Togun, H. S. Sultan Aljibori, N. Biswas, H. I. Mohammed, A. M. Sadeq, F. L Rashid, T. Abdulrazzaq, S. A Zearah, *Renewable Sustainable Energy Rev.* **2024**, *203*, 114732.
[104] A. J Niri, G. A. Poelzer, S. E. Zhang, J. Rosenkranz, M. Pettersson, Y. Ghorbani, *Renewable Sustainable Energy Rev.* **2024**, *191*, 114176.
[105] Z. M. Ali, M. Calasan, F. H. Gandoman, F. Jurado, S. H. E. Abdel Aleem, *Ain Shams Eng. J.* **2024**, *15*, 102442.
[106] R. Guo, F. Wang, M. Akbar Rhamdhani, Y. Xu, W. Shen, *J. Energy Chem.* **2024**, *92*, 648.
[107] Y. Yang, Z. Wu, J. Yao, T. Guo, F. Yang, Z. Zhang, J. Ren, L. Jiang, B. Li, *Energy Rev.* **2024**, *3*, 100068.
[108] M. Sajjad, J. Zhang, S. Zhang, J. Zhou, Z. Mao, Z. Chen, *Chem. Rec.* **2024**, *24*, 202300315.
[109] T.-Y. Lin, Y. Chiu, C.-H. Chen, L. Ji, *Geoenergy Sci. Eng.* **2025**, *247*, 213665.
[110] X. Chen, Q. Fu, C.-P. Chang, *Energy Econ.* **2021**, *95*, 105136.
[111] H. Ahmad, A. A. Markina, M. V. Porotnikov, F. Ahmad, *IOP Conf. Ser.: Mater. Sci. Eng.* **2020**, *971*, 032011.
[112] K.-S. Kim, K.-M. Bae, S.-Y. Oh, M.-K. Seo, C.-G. Kang, S.-J. Park, *Elastomers Compos.* **2012**, *47*, 65.
[113] A. Kalhor, J. Dykas, K. Rodak, A. Grajcar, *Adv. Sci. Technol. Res. J.* **2024**, *19*, 178.
[114] A. Fotouhi, D. J. Auger, K. Propp, S. Longo, M. Wild, *Renewable Sustainable Energy Rev.* **2016**, *56*, 1008.

Jusef Hassoun is Associated Professor of Physical-Chemistry and Electrochemistry at University of Ferrara, Italy. After graduating in Chemistry at the University of Rome Sapienza he worked in industrial company for 3 years before returning academy to obtain PhD degree in Material Science in the field of advanced lithium-ion batteries in 2009. He has been Assistant Professor at Chemistry Department of the University of Rome from 2011 to 2015, visiting professor at Hanyang University, Seoul, South Korea and Tokyo University of Agriculture and Technology, Tokyo, Japan. He is co-author of more than 210 papers in international journals, book and chapters.

Kento Kimura received his Ph.D. degree in 2018 in polymer electrolyte materials under the supervision of Prof. Yoichi Tominaga at Tokyo University of Agriculture and Technology. He studied as a visiting student at Sapienza University of Rome from 2013 to 2014 under the supervision of Dr. Jusef Hassoun. After graduation, he worked as a battery materials engineer at Murata Manufacturing Co. Ltd. He re-joined Tokyo University of Agriculture and Technology in 2023 as an assistant professor and is working on fundamental research and development of functional polymer materials, especially for energy applications.

Yoichi Tominaga Yoichi Tominaga is a full professor at Tokyo University of Agriculture and Technology. He was a PhD graduate from Professor Hiroyuki Ohno group in 2000. After graduation, he took up an academic position at Tokyo Institute of Technology in 2000, worked as an assistant professor by 2007. In 2003, he worked with Professor Bruno Scrosati at Rome University as a Research Fellow of Ministry of Education, Culture, Sports, Science and Technology of Japan. His research interests include polymeric and composite materials for batteries, biomass, smart and intelligent devices.